# Optimization of Oscillating Body for Vortex Induced Vibrations

Project #: BJSWE10

A Major Qualifying Project Report

Submitted to:

Primary WPI Advisor: Brian James Savilonis

in partial fulfillment for the requirements for the

Degree of Bachelor of Science

Submitted by:

______________________
Daniel Distler

______________________
Benjamin Johnson

______________________
Mathew Kielbasa

______________________
Barton Phinney

______________________
Professor Brian Savilonis
Primary Project Advisor
Date: April 28th, 2011

# ABSTRACT

Energy from vortex induced vibrations harnessed by either wind or water may be a viable source to generate renewable energy. This report investigates the optimization of bluff body cross-sectional shapes for vortex creation. Selection began by using finite element analysis software and comparing the oscillatory lift coefficients of 12 geometric shapes to a basic cylinder. From these 12 shapes, a “T” shape and a “T” shape with circular trailing edges were selected to be compared to the cylinder in water tank testing. The shapes were manufactured using an ABS rapid prototyping machine and tested in a stand utilizing springs for damping and a fluid flow tank system designed by the team. The frequencies and displacements were analyzed revealing that the “T” shapes produced 50% greater forces and 40% greater amplitudes than the cylinder. However, the cylinder produced an 85% higher frequency, which resulted in higher total mechanical energy. This study concluded the “T” shapes should be used for low speed, high torque generators, while the cylinder should be used for high speed, low torque generators, and the energy harnessed for electricity would be dependent upon the efficiency of the generator.

## ACKNOWLEDGEMENT

We would like to extend our thanks to the following individuals and organizations for their continued support and assistance throughout the duration of our project:

- Professor Savilonis for being our project advisor and helping us bring this project to successful completion
- Worcester Polytechnic Institute for providing us with the facilities and resources necessary for conducting out research.

# AUTHORSHIP PAGE

The signatures below verify that work relating to this report was completed collectively. Each section of the final report was completed with the collaboration of all group members signing below. Daniel Distler, Benjamin Johnson, Mathew Kielbasa, and Barton Phinney each contributed equal efforts in the research, writing, and editing of the final report.

_______________________
Daniel Distler

_______________________
Benjamin Johnson

_______________________
Mathew Kielbasa

_______________________
Barton Phinney

# TABLE OF CONTENTS

# LIST OF FIGURES

## LIST OF TABLES

# EXECUTIVE SUMMARY

The purpose of this project was to maximize the hypothetical energy that could be harnessed from vortex induced vibrations as a form of alternative energy. The objective was to maximize the displacement amplitudes that are produced by a bluff body, which is oscillating as a result of the induced vibrations. This was done by experimenting with the cross-sectional shape of the bluff body. It was hypothesized that obtaining larger amplitudes would result in a larger amount of work done on a generator, which would result in more energy that could be harnessed to produce electricity. Under this assumption, the shape that produced the largest amplitudes would hypothetically produce the largest amount of energy. Traditionally, a circular shape (i.e. cylinder) is used in flow models to demonstrate vortices, and therefore, it was used as a control for the experiments. The study started by using FEA analysis to determine which shapes would generate the largest lift coefficient. This parameter would provide the largest lift forces and, in theory, the largest amplitudes. From these shapes, three were selected to be manufactured for physical testing in a specially made, small scale test tank.

In order to determine which shapes would produce the largest lift coefficients, FEA tests using Ansys Fluent were conducted using a variety of basic shapes, such as a circle, square, triangle, T-shape, and ellipse, to narrow down to one shape that would be experimented with. These tests were conducted using a Reynold's number range from 100-5000. From the basic shapes, it was found that the T-shape produced the largest lift coefficient, and it was selected to be experimented with for different variations of the shape, such as a circular-T, triangular-T, parachute-T, Y-T and a concave-T. From the FEA

tests with these shapes, which were again conducted with a Reynold's number range from 100-5000, it was found that the concave-T shape produced the largest lift-coefficient. Therefore, this shape was selected to be manufactured for the physical testing. The basic T-shape was also selected as a comparison, and the circle was selected as a control.

The three shapes mentioned above were manufactured in bars out of ABS plastic using rapid prototyping. The bars were approximately ten inches long and the characteristic length (i.e. the diameter) was one inch. The bars were vertically attached to a drawer slider which would allow the bars to oscillate due the vortices they produced. Springs were attached to the bars to damp the oscillations and allow for damped driven oscillations. The slider was attached to a piece of plywood that was the approximate width of the channel of the test tank. The test tank consisted of an oval metal tank that was six feet long by two feet tall by two feet wide. A flow channel was constructed that was approximately a foot wide by a foot tall by four feet long. The channel was placed in the center of the tank with approximately six inches on either side. At one end of the tank, three sump pumps were placed: two pumps of one half horsepower and one of one third horse power. The outlet of each one half horse power pump was directed on the outside of each side of the channel, while the outlet of the one third horsepower pump was split equally on either side of the channel using PVC pipe. A converger was put at the other end of the tank, which converged the flows on the outside of channel and redirected them inside the channel. This created a circular flow in which the flow traveled around the outside of the channel and then through the middle of the channel.

By using the three pumps, three different speeds were used to test the three vertical bars. The bars were submerged in just under a foot of water in the test tank. The concave-T had the largest amplitudes and forces of the three shapes, while the T-shape had the second largest amplitudes and forces. The circle had the smallest amplitudes and forces, which were much smaller than the other two shapes. It also failed to constantly oscillate, which may have been due to an inability to obtain the proper lock-in frequency as a result of the springs used for damping. The concave-T had the smallest frequency, and the T-shape had the second smallest frequency. The circle had a much larger frequency than the other two shapes, and because of this feature, it was determined the circle had the highest power density. However, it is difficult to say which shape would perform better for power production since the T-shapes could produce more power per period given the high forces and amplitudes, while the circle could produce more power over time given its shorter period.

Further work in this area should include research into increasing the scale of testing, and achieving the lock-in frequency for all test pieces. These changes will increase the validity of the data collected and may lead to more conclusive paths to continue work. One additional recommendation for future studies in this area is to consider the type of generator being used to extract power from the system. The properties of the generator will highly influence the optimal design of the oscillating body. Energy generation from vortex induced vibrations had tremendous potential if continued investigations optimize both the shape of the oscillating body and the efficiency of the entire system when including the generator.

# 1. Introduction

As the earth's population increases and becomes more modernized, it has become evident that supplying energy to everyone is a daunting task. Furthermore, the resources used to supply this energy, generally fossil fuels, do not regenerate at a rate to consider them renewable. The United States gets approximately 93% of its energy from nonrenewable sources. These sources include uranium ore (nuclear), coal, natural gas, and oil (U.S. Energy Information Administration). As we drain the supplies of earth's resources, we must figure out a way to create energy using renewable sources. In recent years, interest has been shown in the field of renewable energy generation using sources such as solar panels, hydroelectric dams, hydrogen fuel cells, biofuels, and arguably the most well-known, wind turbines.

"In 2009, wind machines in the United States generated a total of about 71 billion kilowatt-hours, about 1.8% of total U.S. electricity generation." (U.S. Energy Information Administration) Wind turbines are a renewable energy source that requires the flow of a fluid over its blades. As wind, the fluid, flows over the blades of a turbine, an airfoil profile incorporated into the blade will generate lift which spins the blade. The blade is attached to a turbine and

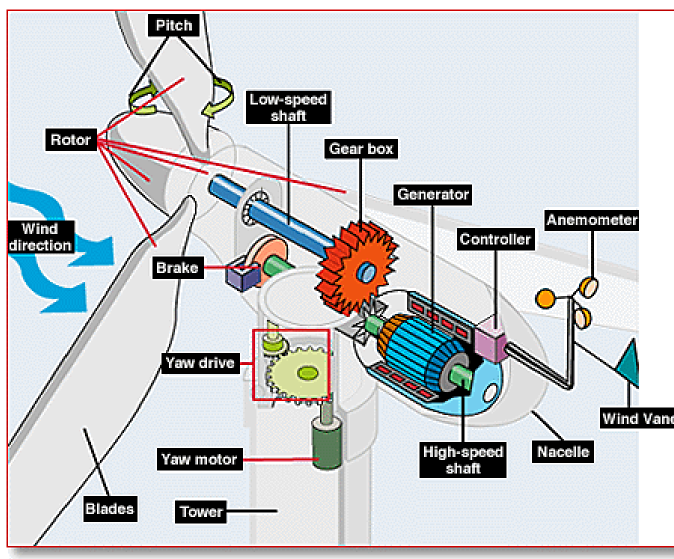


Figure 1: Schematic of a large wind turbine (U.S. Energy Information Administration)

generator so the torque that the blade rotation creates leads to the energy generation. Wind is a source that cannot be depleted.  Figure 1 shows the basic components of a large wind turbine.  The driving mechanism for wind is the sun.  As long as the sun shines, the wind will be blowing at some point.  The largest problem with wind turbines is that the velocity of wind that is needed to power a wind turbine at an efficient economical rate is not as abundant as some may believe.  In some areas with regular high wind velocities, large wind turbines are ideal as long as the obvious visual impact is tolerable. Unfortunately, the area where this is possible is much lower that the population may believe.  Figure 2 gives a fairly detailed depiction of wind tendencies across the United States.  Although smaller turbines can operate in much smaller wind velocities, they cannot produce the torque that is required to make them economically worthwhile.

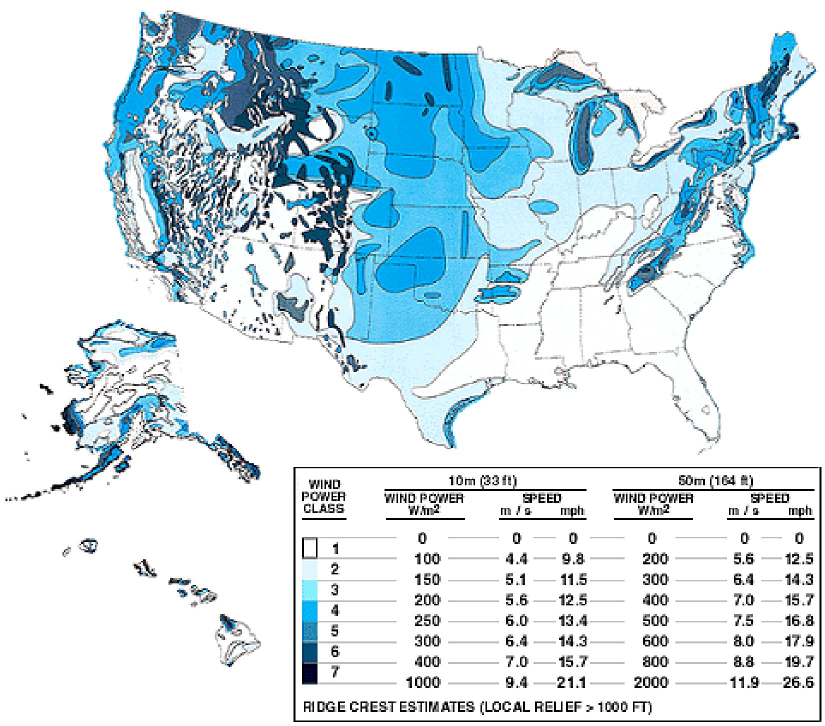


Figure 2: United States Wind Map Diagram (U.S. Energy Information Administration)

This Major Qualifying Project will further research that has occurred in the field of vortex shedding and energy generation that is produced from vortex induced vibration.  As fluid flows over a bluff body at a specific velocity range; vortices will be shed off of the body’s trailing edge.

The shedding of these vortices will lead to vibrations in the bluff body. If the body has 1 degree of freedom in the direction of the vibrations, it will oscillate up and down at a specific frequency, and lead to energy generation. This oscillation will lead to energy generation. This concept is best demonstrated in the newly implemented VIVACE converter developed by Vortex Hydro Energy (Vortex Hydro Energy, 2010). Its cylinders oscillate in Michigan's St Lawrence River at water speeds as low as 2 to 4 knots. This velocity was sought after because most turbine technology cannot function in fewer than 4 knots, while most currents in the rivers and oceans of the United States are less than 3 knots.

With greater research in this field, more applications for this technology can be developed. Further inquiry into the shape of the oscillating body could prove to be beneficial in vortex development, frequency, and strength, in this study. A wide range of bluff bodies will be studied including a "T-shape", a delta, an oval, and a crescent, while the cylinder will also be tested as a control. With successful development of a more efficient vortex generator, it may even be possible to apply concepts learned in this study to air flow, an area much harder to generate power in due to its significantly lower energy density.

# 2. Background

In order to fully understand the principle of generating energy through vortex induced vibrations, there must be a deeper understanding of the forces involved. This background will introduce vortices, their causes, their behavior in varying fluid flow, and the repercussions of vortex generation. Past research in the field of vortex induced vibrations will be discussed. Finally, the positive environmental impacts of this type of energy generation and the available energy in water will be examined.

## 2.1. Cause of Vortices

All real fluids have a shear viscosity that is greater than zero, and a fluid with a shear viscosity of zero is an idealized fluid used for simplifying calculations. Since all fluids possess some shear viscosity, as a fluid flows over a rigid body, a boundary layer of fluid is created at the surface of the body (Wu, Ma, & Zhou, 2006, p. 2). A boundary layer can be defined as a "thin layer of fluid adjacent to the surface of the structure through which the flow velocity increases from 0 at the surface to the free stream velocity at the outer edge of the boundary layer." (Green, 1995, p. 534). Shear stresses are a result of these boundary layers, which cause a rotational flow where the boundary layer separates from the rigid body. These rotational flows are what make up vortices, and have a very high concentration of energy. Given certain Reynolds numbers, the concentrated vortices will interact with one another, becoming unstable and create turbulence (Wu, Ma, & Zhou, 2006, p. 2).

Vortices can be categorized by 3 separate types. These types include forced (or rotational) vortices, free (or irrotational) vortices, and combined vortices (Wu, Ma, & Zhou, 2006, pp. 302 - 303). Forced vortices occur when a liquid tank is spun around its central axis. When this occurs at a certain angular velocity, the tangential velocity of the rotating fluid is proportional to the distance from the central axis (vortex's core). In this case, the rotating fluid can be looked at as a rigid body rotating about its central axis. The speed of the fluid at the center of vortices of this type will be zero.

The next type of vortex that exists is a free or irrotational vortex (Wu, Ma, & Zhou, 2006, pp. 302 - 303). These are most commonly seen when draining a sink or bathtub. For this type of vortex, the tangential velocity of the fluid is inversely proportional to the distance from the axis of rotation. Fluid farther from the vortex core will be rotating slower than that nearer to the core. For free vortices, the angular velocity is greatest at the center.

Combined vortices often form naturally. A combined vortex consists of a forced vortex 'trapped' inside of a free or irritation vortex (Wu, Ma, & Zhou, 2006, pp. 302 - 303). The center part of the vortex is behaving as a forced vortex, but the 'tank' that it is within is a free vortex. This spinning free vortex causes the inner part to spin and therefore it acts as a forces vortex.

## 2.2. Vortex Shedding

Vortex shedding is determined by two properties; the viscosity of the fluid passing over a bluff body, and the Reynolds number of that fluid flow. The Reynolds number relates inertial forces to the viscous forces of fluid flow (Water Flow in Tubes - Reynolds Number). In higher Reynolds number regions, inertial forces dominate the flow and turbulence is found, while in low Reynolds number regions, viscous forces dominate the flow and laminar flow is developed. The creation of strong clean vortices occurs in lower Reynolds number regions. When flow separates from the trailing edge of a submerged body, a region of extreme low pressure will occur because of viscous effects (Georgia Tech). A vortex will form in this area of extreme low pressure to create pressure equilibrium. As fluid flow over the bluff body continues, disturbances will cause the vortex to be “shed” from the trailing edge of the submerged body. Again, a low pressure region will be created and the previous process will continue.

“Vortex shedding can induce damaging large amplitude vibrations of flexible structures in fluid flows and produce intense acoustic pressures in ducts.” (Green, 1995, p. 533). The frequency of vortex shedding is a function of the Strouhal number which relates the frequency to the free stream velocity and cylinder diameter (Georgia Tech). Through testing it has been accepted that the Strouhal number is 2.1 for a wide range of Reynolds number, for infinitely long circular cylinders. The fact that the Strouhal number is so consistent allows the frequency of vortex shedding to be used as the basis for the design of fluid flow meters (Green, 1995, p. 541).

At higher Reynolds numbers, vortex shedding varies over a narrow band of frequencies, with varying amplitudes, and also varies along the span of a submerged, stationary cylinder (Green, 1995, p. 541). Pressure oscillations that occur in Reynolds numbers under 400 tend to be the strongest (Georgia Tech). The strong oscillations lead to the formation of a Kármán Vortex Street. Reynolds numbers greater than 400 entail street destruction due to turbulence. This meaning the flow will not be straight, and there will be disruptions in the flow.

### 2.2.1. Von *Kármán* Vortex Street

A von Kármán vortex street is the description given to an alternating pattern of vortices. When a fluid flows over a blunt, 2 dimensional body, vortices are created and shed in an alternating fashion on the top and bottom of the body (Graebel, 2007, p. 103). Given that the body is symmetrical, this phenomenon will initially be symmetrical but will eventually turn into the classical alternating pattern. Figure 3 is a good depiction of a common von Kármán vortex street. This behavior was named after Theodore Von Kármán for his studies in the field.

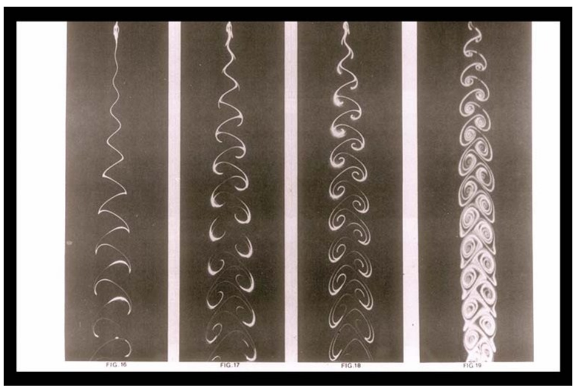

Figure 3: Von Kármán Vortex Street at increasing Reynolds Numbers (Green, 1995, p. 537)

"Although von Karman's (1912) ideal vortex street has been long associated with the wake of a circular cylinder, the only requirement for the existence of a vortex street is two parallel free shear layers of opposite circulation which are separated by a distance *h.*" (Green, 1995, p. 536). Von Karman calculated that in order for there to be stability in the Karman vortex street, the ration between the vertical distance between the centers of alternating vortices, $h$, and the horizontal distance between the centers of alternating vortices, $l$, ideally should be approximately 0.281.

### 2.2.2. Different Reynolds Number Regions

The behavior of a how a fluid will flow around a rigid object can be related to the Reynolds Number of the fluid flow. The Reynolds number is a unit without dimensions that measures the ratio between inertial forces and viscous forces (Dalton, p. 6). Inertial forces (also known as fictitious forces) are defined in accelerated frames. These frames include straight line (or rectilinear) acceleration, rotational (centrifugal or Coriolis) accelerations, and the fourth is from a changing angular velocity. Viscous forces are dependent on the fluid and temperature. When viscous forces are relatively high, the viscosity is said to be high, denoting a relatively "thick" fluid. For different values of Reynolds numbers, a fluid will flow differently about a rigid body. From previous studies of vortices created behind a cylinder placed in a fluid flow, the following ranges of Reynolds numbers proved to result in the vortices shown in Figure 4.

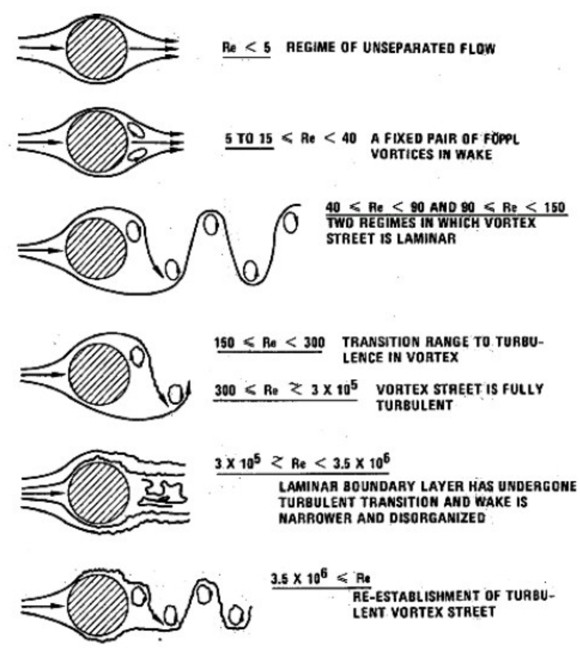


Figure 4: Regions of fluid flow across a smooth circular cylinder (Dalton, p. 6)

The flow patterns observed for different ranges of Reynolds numbers from another study are shown in Table 1 below.

Table 1: Regions of fluid flow across a smooth circular cylinder (Green, 1995, p. 536)

| **Reynolds Number Range:** | **Flow Observations:** |
|---|---|
| **0<Re<5** | Flow follows cylinder contours (no vortices). |
| **5<Re<45** | Flow creates a symmetric pair of vortices. As Re increases in this region, the stream wise length of the vortices will increase up to 3*d at 45) |
| **Re>45** | Flow creates laminar periodic vortex street. |
| **150<Re<300** | Shed vortices become turbulent, Boundary layer along cylinder remains laminar |
| **300<Re<3x105** | Vortex street is fully turbulent |
| **3x105<Re<3.5x106** | Laminar Boundary Layer has undergone turbulent transition. Wake is narrower and disorganized |
| **3.5x106<Re** | Re-establishment of turbulent vortex street |

These two studies returned very similar results. The first study gives more detail for the fluid flow in the range of Reynolds numbers from 45 to 150.

## 2.3. Vortex Induced Vibrations

Vortex induced vibrations occur when the shedding of vortices occurs, alternating on either side of a bluff body. The repeated, alternating shedding of vortices creates a force that is normal to the general direction of flow over the bluff body. This load will alternate, corresponding to the side each vortex is shed from (Hansen, 2007). When the load varies in a harmonic manner at the same frequency as the vortex, vibrations will occur and become stronger. This frequency is a function of the Strouhal number.

Vortex induced vibrations affect everything from small scale heat exchanger tubes to large scale bridges, buildings, and pipes used in offshore drilling (Hansen, 2007). One of the most well-known examples of vortex induced vibrations is the destruction of the Tacoma Narrows Bridge in Washington on November 7th, 1940 (Matsumoto, Shirato, Yagi, Shijo, Fguchi, & Tamaki, 2003, p. 1547) seen in Figure 5. Vibrations become significant when the frequency of vortex shedding is the same as the natural frequency for the bluff body in a cross wind condition (Hansen, 2007). This resonance velocity can be defined as:

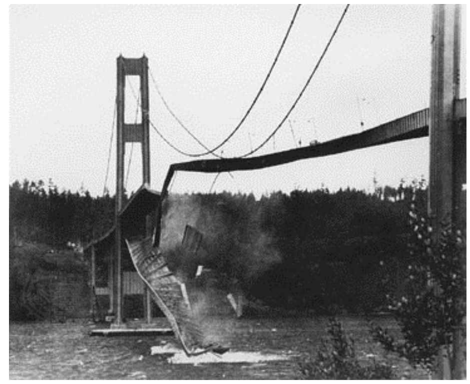

Figure 5: The collapse of the Tacoma Narrows Bridge (Matsumoto, Shirato, Yagi, Shijo, Fguchi, & Tamaki, 2003)

$$v_r = \frac{n_e b_{ref}}{St}$$

Where,
$v_r$ – resonance velocity
$n_e$ – natural frequency
$b_{ref}$ – reference crosswind width
St – Strouhal number

For the Tacoma Narrows Bridge, this resonance velocity was 19 m/s (Matsumoto, Shirato, Yagi, Shijo, Fguchi, & Tamaki, 2003, p. 1547).

### 2.3.1. Influence of Vortex Shedding on Vortex Induced Vibrations

Due to vortex shedding essentially being a sinusoidal process, it is possible to model the lift from vortex induced vibrations as a force that oscillates harmonically (Green, 1995, p. 546). This force can be described as:

$$F_L = \frac{1}{2}\rho U^2 D C_L \sin(\omega_s t - \varphi)$$

Where,
$F_L$ –> Force of vortex induced lift
$\rho$ –> fluid density
U –> free stream velocity
D –> diameter or characteristic length
$C_L$ –> lift coefficient
$\omega_s = 2\pi f_s$ –> circular vortex shedding frequency
t - > time
$f_s$ -> vortex shedding frequency

When a submerged cylinder vibrates normal to the free stream direction at the vortex shedding frequency, or relatively close, the vibrations can cause four main reactions (Green, 1995, p. 542) First, the strength of the shed vortices increase, altering the phase, sequence and pattern of vortices in the wake. Secondly, the wake may become more correlated across the span of the bluff body. The third reaction is that the average drag may increase.

The fourth reaction is more significant. As the frequency of the vortex shedding becomes closer to the cylinder's vibration frequency, "lock-in" or "synchronization" occurs (Green, 1995, p. 542). The "lock-in band" is the range of frequencies where the vortex shedding frequency is controlled by the vibration frequency of the cylinder. As flow is adjusted so that the shedding frequency approaches the natural frequency; the vortex shedding frequency will "lock" onto the structure's natural frequency. This will lead to produce vibrations in the structure (Green, 1995, p. 545). When the vortex wake oscillates in a resonating fashion, significant amounts of energy will be applied to the structure. The range of velocities that will produce this phenomenon can be described as:

$$4 < \frac{U}{f_n D} < 8$$

Where,
U = free stream velocity of fluid
$f_n$ = natural frequency
D = diameter or characteristic length

This can also occur if the cylinder's frequency of vibration is a multiple or sub-multiple of the frequency of vortex shedding (Green, 1995, p. 542). Additionally, submerged cylinders are not the only bluff body shapes where "lock-in" occurs.

## 2.4. Different Bluff Body Shapes

The shape of the bluff body in a stream determines how efficiently it will form vortices. This efficiency primarily depends on how easily vortices are generated, how big they are, and how large the frequency is, which is determined by the Strouhal number (El Wahed, Johnson, & Sproston, 1993). A study was performed in the early 1990's by the University of Liverpool to analyze the effect that different shaped bluff have on vortex shedding. The purpose of the study was to optimize the performance of flow meters by designing a bluff body which generates vortices over a wide variety of Reynolds numbers. The study used five cylinders with different cross sections: circular, trapezoidal, triangular, rectangular, and T-shaped. The study then tested the cylinders with a computer simulation program in a flow with a Reynolds number of around 9125. Of the five cylinders tested, the

T-Shape cylinder produced the strongest vortices. The study concluded that this was due to the “splitter plate” of the T-Shape that helped create a clear signal.

A patent for a T-shaped flow meter also provides data on frequencies and oscillations with respect to the ration of length to width. When this ratio is equal to zero, the frequency is unstable and keeps changing for all Reynolds numbers between 2,000 and 35000 (Chou, Miau, Yang, & Chen, 1994). This instability remains the case until the ratio reaches 1.56. At this ratio, steady oscillations occur up until a ratio of 2.0 with the frequency being larger closest to the ratio value of 1.56. After a ratio of 2.0, the oscillations become unstable again. However, the magnitude of the frequency decreases as the length/width ratio increases.

Another such study focused on just a triangle shape and a T-shape, but also reversed the flow such that the point of each object faced into the flow (Merzkirch, 2005). The study used a flow varying from 2 m/s to 30 m/s which resulted in Reynolds’s numbers from 13,000 to 195,000. The width of the triangle bluff body was 24 mm, while the width of the T-shaped body was 10 mm. With the flat side of the triangle into the flow, the frequency that was produced was 6.7 Hz and a Strouhal number of .16, while with the tip into the flow produced a frequency of 14 Hz and a Strouhal number of .34. With the flat side of the T-shape into the flow, the frequency that was produced was 12 Hz and a Strouhal number of .12, while with the tip into the flow produced a frequency of 20 Hz and a Strouhal number of .2. Scaling the T-shape down to the size of the triangular shedder, the frequencies obtained for the flat edge into the flow and the point into the flow are 5 Hz and 8.3 Hz, respectively. This means that the triangular shape with the point into the flow would

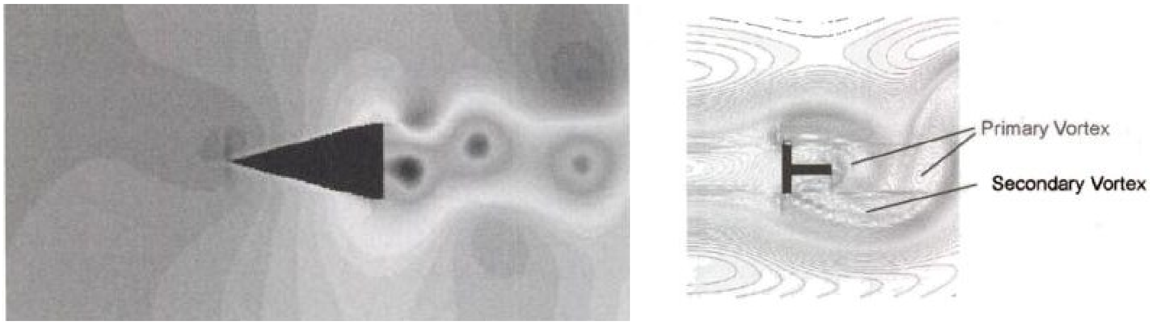

Figure 7: Triangular (left) and T-shaped (right) vortex shedders (Merzkirch, 2005)

produce the highest frequencies. This data suggests that for obtaining a steady, constant oscillation, a T-shaped cylinder should be used. However, the T-shape cylinder does not appear to reach as high a frequency as other shapes might, which means that although it is arguably the most consistent, it may not produce the most energy. The triangle and T-shape bluff bodies are shown in Figure 7.

## 2.5. Past Research

There have been many studies of vortex induced vibrations for cylinders. These case studies will give a basis for the ideas that are trying to be accomplished in this project. They provide techniques and test data that will be helpful later on in the testing of the project. For the first study involves a professor from the University of Michigan. And the second is a study conducted by a doctoral student at the California Institute of Technology.

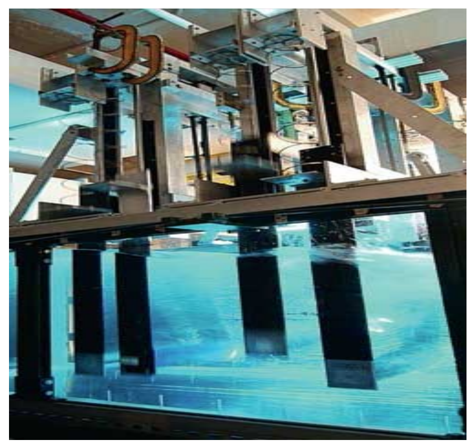
Figure 6: Setup of tank and cylinders for the University of Michigan study (Vortex Hydro Energy, 2010)

### 2.5.1. Case Study I: University of Michigan

The study conducted was done by Professor Michael Bernitsas, who is head of the Marine Renewable Energy Lab at the University of Michigan at Ann Arbor, and three other doctorate students (Bernitas, Raghavan, Ben-Simon, & Garcia, 2008). The study conducted was for high Reynolds Number around 1,000,000. The experiment was performed in a large tank, and four cylinders were immersed in the tank. Each cylinder was 36 inches in length and 3.5 inches in diameter. The Test tank can be seen in Figure 6.

The fluid velocity created was 2.6 knots, which is about 1.3 meters per second (Bernitas, Raghavan, Ben-Simon, & Garcia, 2008). The cylinders are attached to springs which allow them to move up and down freely, from the current. The springs had a stiffness value of 518 N/m. The Reynolds Number for the test ranged from 0.44 x $10^5$ to 1.33 x $10^5$. A rotary electrical generator was used to convert the energy harnessed into electricity. The experimental results were not available. However, Professor Bernitsas wrote that the system worked as expected and the energy was harnessed and converted using the electrical converter. Figure 8 shows the setup of the generator, and how it was setup in order to convert the energy into electricity.

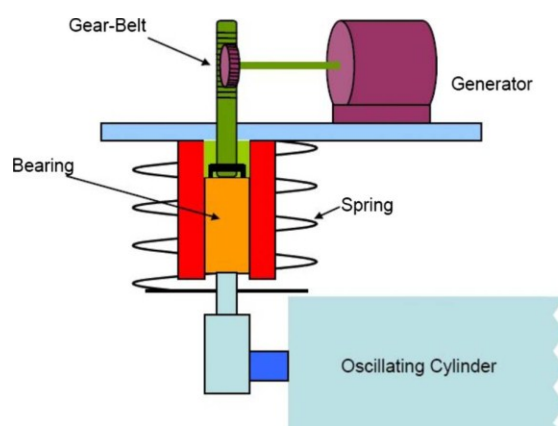

Figure 8: Energy generation unit from the University of Michigan study (Madrigal, 2008)

Professor Bernitsas has also developed a company around this concept called Vortex Hydro Energy. They are in the process of doing large scale testing, in actual under water environment in the Detroit River. This is expected to be done within the year.

### 2.5.2. Case Study II: California Institute of Technology

This system was setup differently than the University of Michigan study and was used for finding the effects of damping and Reynolds number on vortex induced vibrations (Klamo, 2007). The setup used was for much smaller scale testing, and was elastically-mounted rigid circular cylinder, free to oscillate only transverse to the flow direction, with very low inherent damping. A magnetic eddy-current damping system was installed to be able to limit the damping effects. The range of Reynolds Number used was between $200 \leq Re \leq 5050$. Figure 9 shows the experimental setup used. The flow velocities were varied, and the data was recorded by using a LabView program. For a system with low mass the system proved to have a constant frequency. As the Reynolds Number increased the frequency was not consistent.

Figure 9: Setup for California Institute of Technology study (Klamo, 2007)

## 2.6. Theory and Equations

The theory used for this project is based on flow past a circular cylinder. As the flow moves across the cylinder, it is lifted because of the lift force, which creates the vortex. The equation for the lift force for a non-rotating cylinder is:

$$C_L = \frac{2F_L}{\rho D l U^2}$$

Where:
$F_L$ = Lift Force
$C_L$ = Coefficient of Lift
$\rho$ = Density of the fluid
D = Diameter or characteristic length
l = Length of cylinder
U = Fluid Velocity

The drag force is also an important factor in determining the most efficient sliding design mechanism. The drag force will come from the current of the water and act as the normal force when finding the frictional force. The drag force can be represented by the following equation:

$$C_D = \frac{2F_D}{\rho A U^2}$$

Where:
$C_D$ = Coefficient of Drag
$F_D$ = Force of Drag

The lift force, above, is dependent on the Reynolds Number. The Reynolds Number gives a relationship between the density, velocity of fluid, diameter of cylinder, and the viscosity of the cylinder.

The Reynolds Number can be calculated by the following equation:

$$Re = \frac{\rho D U}{\mu}$$

Where:
Re = Reynolds Number
$\mu$ = Viscosity of Fluid
$D_H$ = Hydraulic Diameter

An equation for the coefficients was first derived, and then used to solve for the drag and lift forces, using the Reynolds Number.

The Strouhal Number is also an important that is used when calculating the frequency of the oscillation for the cylinder, as it moves up and down. The Strouhal Number can be represented as

$$St = \frac{\omega D}{U}$$

Where:
St = Strouhal Number
$\omega$ = Frequency of oscillation

To calculate the frequency of oscillation, the equation below is used.

$$\omega = \sqrt{\frac{C_L \rho U^2 A}{2m4x}}$$

Where:
A = Area
m = mass
x = amplitude

These are the main equations behind the theory of the vortex induced by vibrations (White, 2011). They will be used in the design phase more to calculate the lift and the frequency for a given velocity. The velocities used will be used to demonstrate flow from a current in a natural body of water, such as a river. From here the Strouhal number can then be compared to the Reynolds number and see the how the two are affected.

## 2.7. Energy in Water

The amount of energy able to be harnessed in flowing water can be calculated using the equation for conservation of energy. If heat transfer is neglected and the flow of the water is assumed to be perpendicular to the control volume such that the full amount of energy can be calculated, the resulting equation is as follows:

$$[(\hat{u} + (\rho/P) + (V^2/2) + gz)\dot{m}]out - [(\hat{u} + (\rho/P) + (V^2/2) + gz)\dot{m}]in = \dot{W}$$

Where:
$\hat{u}$ = enthalpy
$\rho$ = density
P = pressure
V = velocity of the water
g = acceleration due to gravity
z = vertical height
$\dot{m}$ = mass flow rate
$\dot{W}$ = Power

In order to calculate the amount of usable energy, the energy equation must be simplified to look at the kinetic energy of the water. This is accomplished by neglecting changes in enthalpy, pressure, and height, which reduces the equation to:

$$(V^2/2)\dot{m} = \dot{W}$$

However, this power is not the amount of electrical power that can be generated as no generator is a hundred percent efficient. This power must be multiplied by the efficiency of a generator to estimate the total amount of electrical power that may be captured. This equation does not include head loss due to friction since it is for a large body of water where frictional effects may be considered negligible, along with the efficiency of the system.

Today, there are many designs that are used to harness water energy as form of green energy. Most of these devices are turbines that either harness energy from damming a river to increase potential energy or harness energy from natural tides or ocean currents. One issue with these devices is that they require large velocity (around 6 knots) in order to produce useful electricity (Madrigal, 2008). Usually to achieve this flow or more, rivers need be dammed which has a large negative impact on the environment. The largest limitation for tidal energy is the fact that most ocean currents only reach speeds of 3 knots, so areas that have enough flow to justify a tidal generator are scarce (Madrigal, 2008). However, the amount of energy that can be harnessed in either prevailing currents or tidal fluctuations is estimated to be between 280,000 and 700,000 terawatt-hours, which is very large when compared to the worldwide electrical generation figure of 16,000 terawatt-hours (Vortex Hydro Energy, 2010). Needless to say, there is a lot of potential for harnessing water energy.

## 2.8. Positive Environmental Impacts

Current vortex energy projects are able to generate electricity in flows between 2 and 4 knots (Vortex Hydro Energy, 2010). Given that this is about half the flow needed by conventional hydroelectric devices, not only is there a greater energy market, but it does not require the damming of rivers. Damming rivers can have an extreme negative impact to the surrounding environment. The area above the dam is completely flooded resulting in a loss of habitat and the area below the dam is starved for water. Damming significantly reduces the environmental benefit of using hydro power. Since current devices do not require damming of rivers, they are very environmentally friendly. They also use renewably energy, have no emissions, and are relatively small compared to conventional hydro generators meaning they are unobtrusive to aquatic life. Fish use the vortices to propel themselves forward and be able to swim in schools.

# 3. Design Process

## 3.1. Test Tank Design

Designing the test tank took presented many challenges. The main goal that proved difficult to accomplish was to achieve an even flow profile. The design that we finally choose to build uses two circular flows of water, merging together into a diffuser, followed by the testing area.

Preliminary designs included using a single oval or circular-shaped flow channel. Figure 10 below is a preliminary sketch of this single oval-shaped flow design estimated to cost $150.

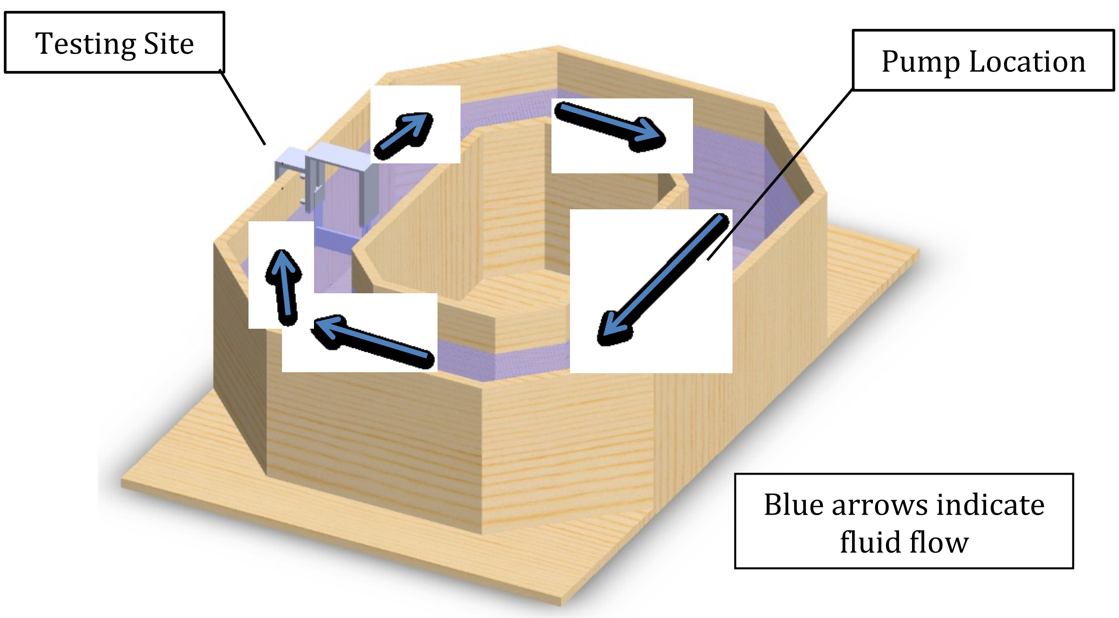


Figure 10: Oval Flow Circular Design

After farther research, the team realized that this design would result in faster flow velocities on the outer perimeter of the circular flow and slower flow velocities at the inner perimeter. Since a relatively even flow profile was desired, this design was not accepted.

Another preliminary design was to use two pools of water. With this design, a pump would pump water from the lower pool to the upper pool. The upper pool would drain and be channeled through an area with a suitable cross section (the test area) and drain into the lower pool, where the pumps could bring it back to the upper pool. After doing calculations to find achievable flow rates with this design, we found out a massive pump or pumps would be required to achieve a steady, continuous flow. The pump required for this design would need to be on the scale of pumps used in recreational water parks for large multi-person waterslides. Utilizing such a pump would not at all be an economical way to achieve the desired flow. One alternative was to design the test tank to have the desirable flow for the time that it takes for the water to drain from one tank to the other, a non-continuous flow. A major problem with this is that a steady continuous flow would be very advantageous for testing purposes. Additionally, as the upper tank drains, the pressure at the drain of the upper tank will be decreasing. This is due to the fact that pressure at a depth, h, below a free surface can be calculated by multiplying the specific weight of the fluid by the value 'h' ($Pressure = h * spec.weight$). Since 'h' is decreasing as the water drains, the pressure at the drain is decreasing over time. Since the pressure head at the drain is proportional to the fluid pressure, the head will be decreasing as well. The pressure head decreasing means the flow rate out of the drain will be decreasing. With this design, the flow rate out of the drain is equal to the flow rate through the test area. Since a steady flow rate is desired, this is another flaw in this design, thus iteration was necessary.

The next design that we considered was to create 2 circular flows separating at one end and merging together at the other end. The original method of creating water flow was going to be a propeller. We considered using an electric trolling motor, or building something similar using a propeller, electric motor and a chain. Figure 11 shows a preliminary CAD model of this design.

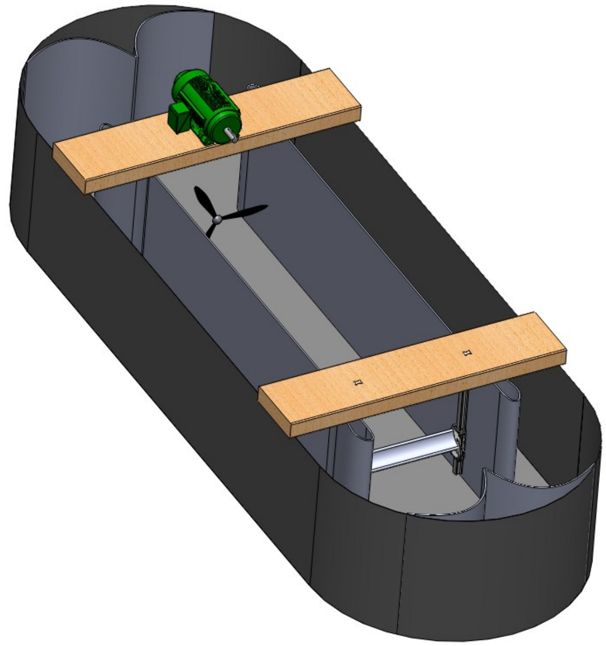

Figure 11: A SolidWorks Model of a Preliminary Tank Design

However, the team realized that using a propeller to push the water will create a very turbulent flow from the prop wash, and therefore the propeller could not be located anywhere near the test area. To rectify this problem, the team considered using 2 motors with 2 propellers, but instead of placing them in the main flow channel (where testing will occur), they would be placed facing the other direction in the return channels. This way they would push water towards the converger, the water would merge and be forced to go down the main channel, where testing could be performed. However, due to the cost of trolling motors and the time restriction for the project, we did not end up using open propellers to create the water flow.

The method that we ended up following through with is very similar to the design described above; however instead of utilizing propellers, sump pumps that the team had access to were used. PVC piping was connected to the outlets of the pumps and directed the water flow properly. This can be shown in Figure 15 (Page 43).

The flowing water converges at the end, and then returns down the center test channel. While it is not perfect, this design produced a fairly uniform flow. Additionally, the use of a diffuser helped to make the flow more laminar. Figure 12 shows the diffuser built from various PVC pipes.

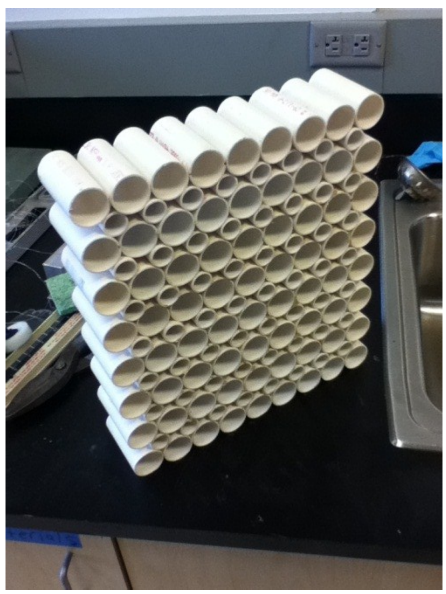

Figure 12: The Diffuser

## 3.2. Sliding Mechanism/Prototype Design

Designing the sliding mechanism took several iterations as well. The main goals were to constrain the shape's motion to one degree of freedom, keep the shape's front face perpendicular to the flow, and to keep sliding frictional forces at a minimum. The three design considerations are discussed below.

### 3.2.1. Linear Guide/Bearing Sliding Prototype

Initially, we thought using 2 linear bearings and sliding pucks would be a good method to allow oscillations. Figure 13 shows a CAD model of the general idea.

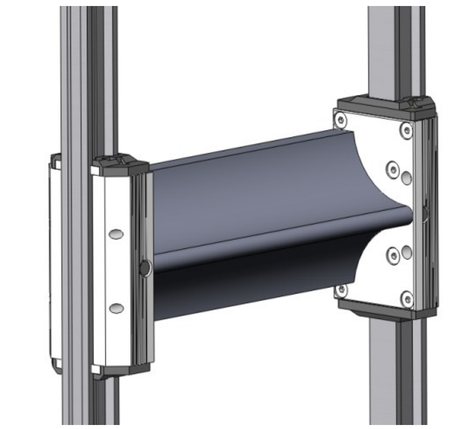

Figure 13: A SolidWorks screen shot shows the T-Shape installed on linear guides

This design can also be seen in APPENDIX B installed on a preliminary design of the test tank, as well as a general plan for how this design of the test tank would work. We never ended up attempting to build this design due to prices of linear guides and sliding pucks. Another disadvantageous part of this design was the fact that the pucks would be underwater for their entire operating life, and it was assumed that the bearings in the pucks would probably not be too efficient if they were constantly running underwater. As a result of this, we attempted to redesign this in a way that keeps the bearings out of the water.

In this design there would be sliding rods and stationary linear bearings. This was the first design that we actually built to attempt oscillations. The general concept is there are 2 rods that pass through stationary linear bearings and connect to the bluff body. The rods and bluff body would oscillate together vertically and perpendicular to the direction of water flow. A block of aluminum was machined to allow the bearings to drop into place with a set screw to assure the bearings do not move during operation. Through holes were also drilled in this block to bolt it in place. This design can be seen in Figure 14.

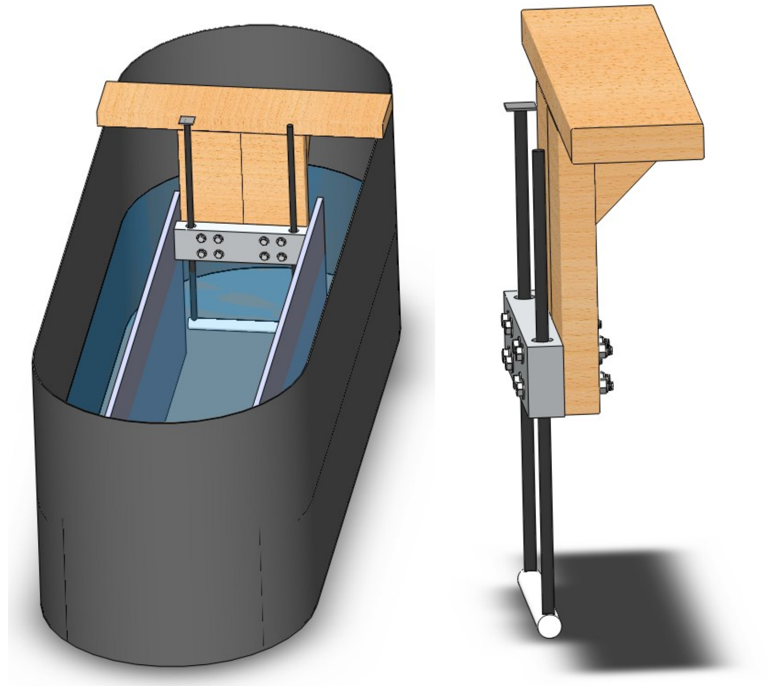

Figure 14: Vertical Rod / Linear Bearing Design

Material selection for the sliding rods took several factors into consideration. We knew that the different shaped bodies we were testing were made of acrylonitrile butadiene styrene (ABS) plastic. These shapes were made of ABS as a result of the availability of WPI's rapid prototyping machine, which utilizes ABS to print 3D geometries. ABS has a density slightly less than water which was good because it will be light and also not sink to the bottom (both of which were desirable). The rods will be partially above water, so the weight of them above the water will prevent the shape from floating to the surface. We were looking for a rod that was sold in a half inch diameter, a common diameter for bar stock, and the diameter of the purchased linear bearings. The problem we encountered was that with lighter materials, the Young's Modulus of the material also tended to decrease. Since the approximate flow velocities were known, and the diameters of the shapes were known, we were able to calculate the drag force that the object would feel during the flow. The rods act as cantilever beams, fixed at one end (the bearings) and subject to a load at the free end. The load at the free end is equivalent to the drag force, which can be calculated using $F_D = \frac{1}{2}\rho u^2 C_D A$. In this formula, the drag force is dependent upon $\rho$, the mass density of water; u, the velocity of object relative to the fluid; $C_D$, the drag coefficient for the given shape (value taken from Fluent); and A, the cross-sectional area (facing the fluid flow) of the shape.

With the load on the rods known and the diameter and Young's moduli for several materials known, we searched for a material that was light and strong enough to deflect less than 0.05 inches at a moment arm distance of 12 inches from the bearings (the maximum possible). An example of the calculations performed to find the deflections are shown in APPENDIX C: MATHCAD CALCULATIONS FOR STRESS AND DEFLECTION OF OSCILLATING RODS. Additionally, the stress in the beam was calculated to ensure it would be well below the yield strength to avoid plastic deformation during normal operation. APPENDIX E: A TABLE USED IN THE MATERIAL SELECTION PROCESS FOR THE OSCILLATING RODS was used to help select a material by organizing materials based on cost and material properties. The material selected was Noryl, which is a combination of Polyphenylene Oxide (PPO) and Polystyrene (PS).

Springs were used to support the weight of the oscillating components. The initial displacement of these springs determined the equilibrium position of the test shape; and this initial displacement was chosen so that at equilibrium the test shape would remain in the center of the testing area. The position sensor would be located above the sliding mechanism and would be pointed towards a plate that was secured to one of the rods (as shown in Figure 14 above). After building this prototype and placing it in our test tank, the team discovered that the friction forces from the rods sliding through the bearings were too great. The lift forces generated from the vortices were not great enough to initiate oscillations. We tried sanding the rods and using lubricants to minimize friction forces, but oscillations could not be achieved, therefore a new design was necessary.

### 3.2.2. Horizontally Oscillating Slider Prototype

To eliminate gravity as a factor, we decided to try using horizontal oscillations of the shape. To do this we secured a standard drawer slide to a piece of plywood. We then secured one end of the shape to the sliding component of the drawer slide. To do this we drilled a hole in the end of the ABS plastic shapes and used a self-tapping screw. This design with the pump configuration is shown in Figure 15.

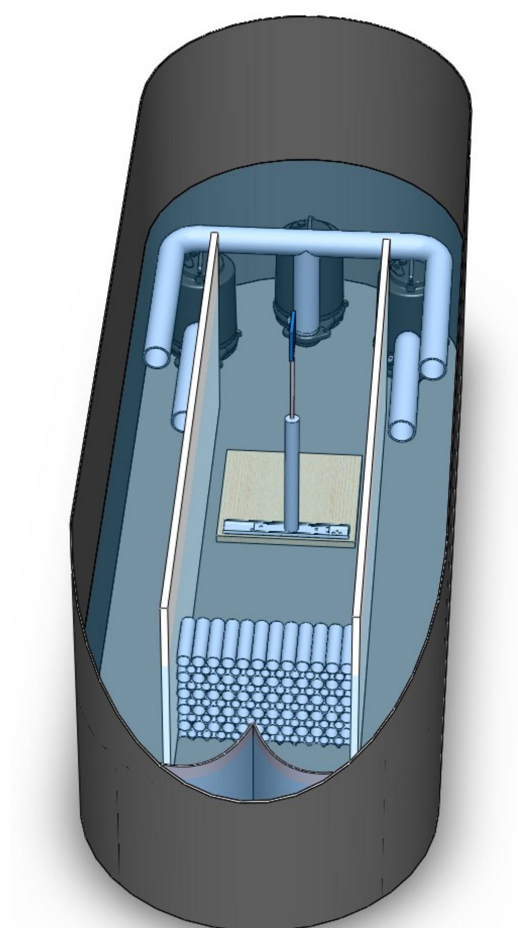

Figure 15: Horizontally Oscillating Design with Pump Configuration

This design proved to work very well. Steady, large oscillations were maintained at even very slow water speeds. To measure the position of the shape, a rod was installed vertically into the top of each shape, with a plate added to the top of it. This plate served as a surface in which the position sensor could easily read its location. The position sensor was suspended from a stand and positioned pointing at this plate. This configuration was used to test all 3 shapes at 3 different flow speeds. This is explained further in the testing methods section and can also be seen in APPENDIX D.

# 4. Methodology

The primary goal of this project was to develop a more efficient cross sectional shape for generating vortices focusing on the lift forces created by the vortices. To do this we also needed to create a water tank capable of variable flow speeds, continual tests, and limited fluid disturbances from wakes, eddies, and inconsistent flow profiles. Additionally, a test stand needed to be developed to allow for oscillations from Vortex Induced Vibrations with as little friction as possible, maximizing the efficiency with hopes for energy generation. Finally, it was important collect enough data to allow for further work in the development of a more efficient collection method, harnessing the higher oscillatory lift forces as a form of renewable energy. The following sections of this report will thoroughly describe the steps taken to reach all of these goals.

## 4.1. ANSYS Fluent Testing Methods

In order to find which general shape would create the highest lift force, FEA tests were first conducted for some basic shapes, which are described later in the methodology, using Ansys 12 Fluent. Initially, trials were conducted by using a diameter of .0254 m (approximately 1 in) and changing the velocity of the water to achieve the desired Reynolds number. This method was chosen for the intent of simulating the small scale physical testing. However, the program was unable to give accurate results due to the large size of the mesh being used. Attempts to use a smaller size mesh required a much longer amount of CPU time to test each shape, which was unacceptable given the time allowed for the study's completion. Therefore, using the test method described below, more accurate results were able to be produced in a more efficient time period.

The FEA tests were conducted using a 2 dimensional geometry in the X and Y directions of the coordinate system and assumed infinite length in the Z direction. The boundaries of the flow field were 20 times the characteristic length (i.e. diameter) high by 30 times the characteristic length wide. This size test area allowed for minimal boundary layer effects on the flow, which was intended to simulate an infinitely wide channel. The shape was positioned at 10 times the characteristic length down from the top, and 10 times the characteristic length to the right of the inlet. The tests were conducted using the following Reynold's numbers: 100, 150, 200, 500, 1000, 2000, 3000, 4000, and 5000. The characteristic length of the shape was kept constant at one meter, and the density property of fluid was varied to achieve the desired Reynold's number. This approach was used because it was most convenient parameter to change to obtain the specific Reynold's number desired, where as changing the velocity, for example, would have taken extra calculations. The flow was set at transient flow with a constant dynamic viscosity of 1 $N*s/m^2$ and a constant velocity of 1 m/s. Once the basic Shapes had been tested, the T-shape was found to have the largest lift coefficient. variations of the T-shape were then tested using the same methods as the basic shape test. The top three variations of the T-shape, as well as the basic T-shape for comparison, were then tested at Reynold's numbers of 6000, 7000, and 8000 in order to determine how each shape would perform under faster flow conditions. The last part of the FEA analysis included testing the shapes at the estimated Reynolds number for the simulated flow of water at operating conditions. The same test method as described above was used except for the following changes to the properties: density was assumed to be 999 $kg/m^3$, dynamic viscosity was assumed to be $1.12*10^{-3}$ $N*s/m^2$, velocity was assumed to be 1.03 m/s (approximately 2 knots), and the diameter was assumed to be .15 m (approximately 6 in). These parameters resulted in a Reynolds number of approximately 140,000.

The basic shapes tested included a square, rectangle, triangle, and ellipse. These shapes can be viewed in Figure (added when known). The varied T-shapes tested included a cylindrical T, a triangular T, a parachute T, a Y T, and a concave T. These shapes can be view in Figure (added when known).The triangle went through two rounds of testing: one round with the point into the flow, and one with point away from the flow. The ellipse went through two round of testing as well: one with the semi-major axis perpendicular with the flow, and one with the semi-major axis perpendicular to the flow. The T-shape was tested with the flat top into the flow. Similarly to the basic T-shape, the variations of T-shapes were tested with the T part facing into the flow.

## 4.2. Test Tank Construction

The test tank was built based around a 6' x 2' x 2' steel, oval water trough to ensure the water holding capacity of the system. The system consisted of a test channel, a diffuser, an oscillation testing stand, a converger, and 3 pumps. The construction, setup, and operation of these subsystems can be found in the following section.

### 4.2.1. Test Channel

Figure 16: Channel for Test Tank

The test channel had a simple construction with three 4 ft. boards of sealed particle board. Two of these boards were 16" wide and were used as the side boards. The bottom board was 11 ¾" wide for the purposes of press fitting the diffuser (see section below) into the channel. The side boards were attached to the bottom board with 4 "L" brackets. After the basic channel was constructed, weather stripping was added around the exposed edges of the front and back while caulking was used as a waterproofing method on the joints. Finally, wooden handles (2" x 2" x 12") were attached across the top of the test channel for removing the channel from the test tank. This allowed the tank to stay filled with water while the test channel could be dried when not in use as seen in Figure 17.

### 4.2.2. Diffuser

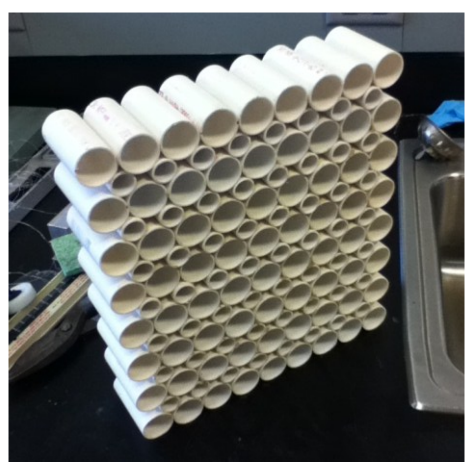

Figure 18: Diffuser for Test Tank

The diffuser was built to create a more uniform velocity profile concentrated around the area where most of our testing occurred. Eliminating turbulence upstream from the testing area provided more repeatable results. We used 18' of 1 ¼" diameter PVC pipe with a wall thickness of 1/16" as well as 14' of ¾" diameter PVC pipe with a wall thickness of 1/16". The PVC pipe was cut into 3" sections. These sections of pipe were glued together using waterproof plumber's glue in the orientation shown in Figure 18.

### 4.2.3. Oscillation Testing Stand

In order to maximize the oscillations, for the test pieces, in terms of amplitude and frequency, a low friction oscillation stand was necessary. To do this, we obtained a sliding drawer rail with metal rails and ball bearings to reduce friction. This rail was cut to 11" in length and was screwed into a square sheet of plywood measuring 11 ½" wide. Attention was paid to mounting the rail parallel to the front edge of the plywood. Doing this ensured that oscillating motion of the bluff body was perpendicular to the free stream velocity of the channel. There is a plate that slides in the rails whose original function was to attach a drawer to the rail. This plate, and two more from two other sets of rails, were removed and attached to the bottom of the oscillating bodies. Attention was paid to mounting the plate parallel to the front face of the oscillating bodies with a flat front face. As with mounting the rail to the plywood, this ensured that the free stream velocity of the channel was perpendicular to the front face of the oscillating bodies. This was less important for the cylindrical oscillating body because it has no flat faces. When we tested each shape, this sliding plate was inserted into the mounted rail. To finish the test stand, a "target" for the motion sensor was attached to the top of the oscillating body. The "target" was made from a piece of cardboard (6" x 6") and an alligator

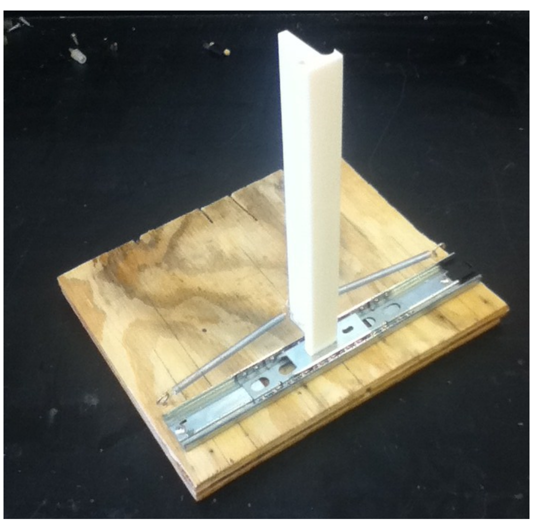

Figure 19: Setup of the Oscillation Testing Stand

clip on a wire that fits into the small hole drilled at the top oscillating body. A picture of the Oscillating Test Stand can be seen in Figure 19.

### 4.2.4. Converger

The converger was used to redirect the flow of the water down the test channel. It was constructed out of thin, pliable sheet metal with each sheet measuring 12" high and 24" long. The converger can be seen in Figure 21 which illustrates the full tank setup. Each half of the converger was initially molded to the ridges in the water trough with a rubber mallet. Caulking was used to seal any other leaks. The converger was connected together after bending the sheet metal in a semicircular fashion, aiming the water down the test channel.

### 4.2.5. Submersible Pumps

To allow for three different flow rates, different combinations or configurations of three submersible pumps were used. The lowest flow rate tested was achieved by turning on 1 central 1/3 horsepower sump pump. This was called "flow rate 1". The 2nd flow rate was achieved by turning on 2 ¼ horsepower sump pumps, utilizing ½ horsepower of sump pumps total ("flow rate 2"). The fastest flow rate tested used all 3 sump pumps (the 2-1/4 horsepower and the 1/3 horsepower pumps) utilizing 5/6 horsepower of sump pumps total ("flow rate 3"). The position of these pumps can be seen in Figure 20.

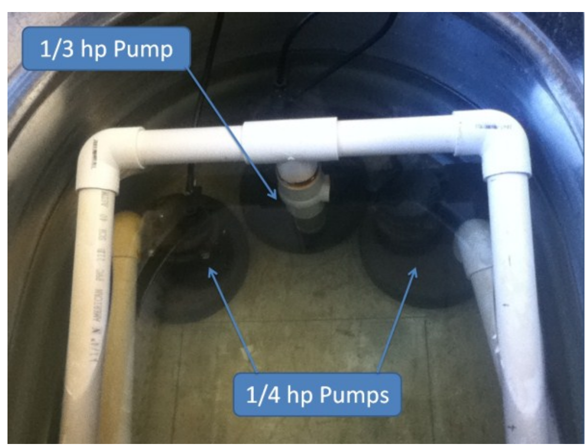

Figure 20: Pump Setup and Configurations

### 4.2.6. Test Tank Setup

Prior to testing, the team secured the test channel in the proper location in the tank. The channel was secured parallel with the sides of the tank and has 5" of clearance on either side for the recirculation channels. The channel should also be centered lengthwise in the tank providing space for the pumps in the rear and the converger in the front. The channel was secured with 5 lb. weights on each side of each support on the protruding screws. Completing the setup of the test tank required assuring that the pumps and converger are in their proper location. After this was completed, the test tank was filled with water up to the top of the converger, creating a depth of 12". Figure 21 illustrates the proper setup of the set tank.

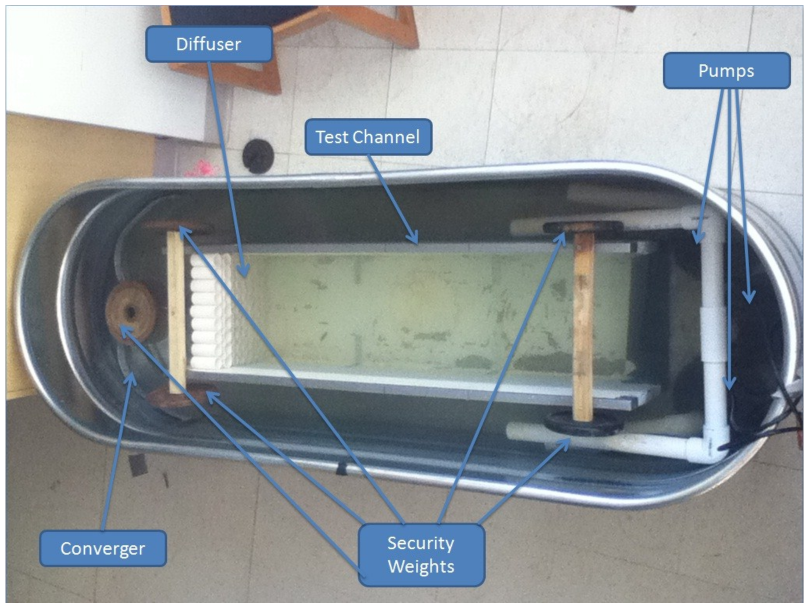


Figure 21: Secured Setup of Tank Elements

**Test Equipment Utilized**

To record the data necessary, several types of testing equipment were utilized. A Vernier LabPro interface (order number: LABPRO) connected the sensors to a computer. The two sensors used plugged into the interface, and the interface was connected to a laptop computer via USB. The first sensor used, a Vernier Flow Rate Sensor (order number: FLO-BTA), determined the flow velocities at certain points in the fluid flow. The second sensor was to determine the position of our cylinders with respect to time. To measure this, a Vernier Motion Detector (order number: MB-BTD) was utilized. Figure 22 **Error! Reference source not found.**shows company photos of the test equipment:

Figure 22: From Left to Right: Vernier LabPro, Flow Rate Sensor, and Motion Detector.

The Vernier LabPro interface was used in conjunction with a laptop through a USB port and the LoggerPro software from Vernier. It has the ability to take 50,000 readings per second and can hold up to 12,000 data points with a 12-bit A/D Conversion.

The Flow Rate Sensor measures the velocity of a fluid by using an impeller. As the fluid passes over the impeller, the impeller rotates, subsequently rotating a bar magnet attached to the impeller's shaft. A read switch monitors the change in the magnetic field as the magnet rotates and converts this signal into a voltage. The output voltage is therefore proportional to the velocity of the fluid and is calibrated with the LabPro interface. When plugged into the Channel 1 input, the Flow Rate Sensor has a resolution of 0.0012 m/s and an accuracy of ±1% of a full scale reading with a velocity range of 0 to 4.0 m/s.

The Motion Detector 2 emits a short ultrasonic pulse from the transducer and registers the time it takes for the pulse to return. By comparing this to the speed of sound in air, the Motion Detector 2 can output the distance to the object causing the echo with a resolution of 1mm and an accuracy of 2 mm. It has a range of 0.15 m to 6 m and an optimal collection rate of 20 samples per second however, it is important that objects within a 15° to 20° cone are removed from the test area to make sure that the proper object is being targeted.

## 4.3. Determining the Velocity Profile at the Test Area

The velocity profile was determined at the test area for the 3 different fluid flow rates. The three different flow rates were created by different combinations of sump pumps. The lowest flow rate (velocity 1) tested was achieved by turning on 1 central 1/3 horsepower sump pump. This will be called flow velocity 1.The 2$^{nd}$ flow rate (velocity 2) was achieved by turning on two ¼ horsepower sump pumps, utilizing ½ horsepower of sump pumps total. The fastest flow rate (velocity 3) tested used all 3 sump pumps (the 2-1/4 horsepower and the 1/3 horsepower pumps) utilizing 5/6 horsepower of sump pumps total. Figure 23 shows the position of these pumps and how their PVC piping was set up.

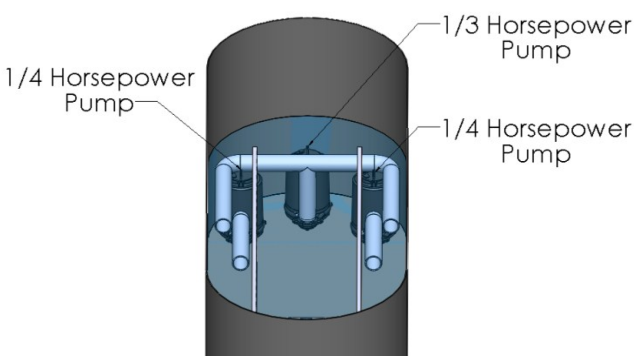


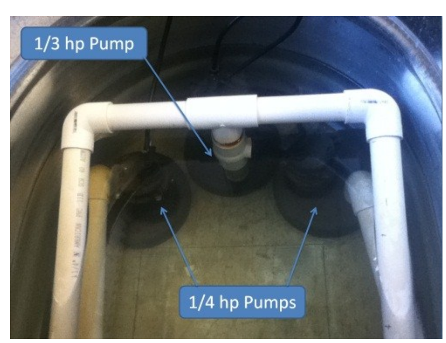


Figure 23: Pump Arrangement with Pumps Labeled (CAD Model and Prototype)

The velocities at 11 chosen positions were measured for each of the pump configurations. To gain the velocity data for each of the 11 position, 500 data points of the velocity were taken over a 20 second time interval. Figure 24**Error! Reference source not found.** shows a layout of the dimensions of these 11 positions with the nomenclature used for each position.

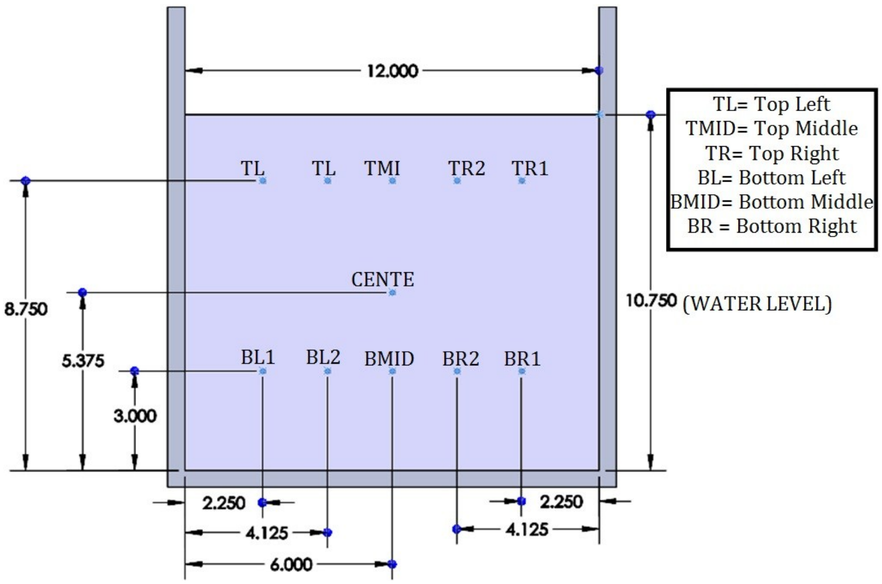


Figure 24: Velocity Profile Locations and Nomenclature

The velocities were measured at each of the 11 locations for each of the 3 flow rates. The velocities were measured 3 times for each location at each flow rate. These three trials were averaged for a given point at a given flow rate to determine an accepted value.

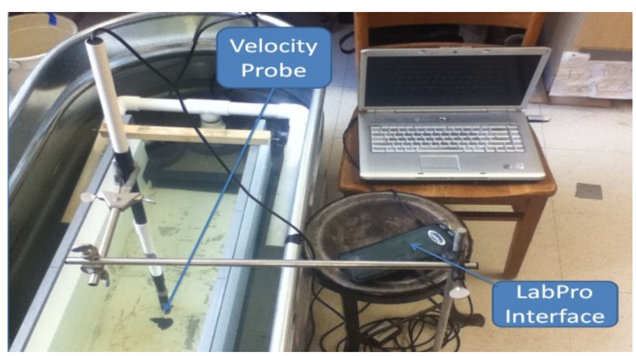


Figure 25: Setup for Velocity Profile Testing

Each trial took the average flow rate over a 20 second interval. Figure 25 shows this test setup.

The data from this testing is shown in the results section on page 76 in tables as well as visual mapped out.

## 4.4. Oscillation Data Recording

After there is a proper flow-profile of the channel, it was time to assemble the bluff body and sliding mechanism. The bluff body test piece was secured to the test stand outside of the tank. A sliding platform with bearings should be secured to the bottom of the bluff body, and that sliding platform should be placed in the bearing rack. Then springs were attached to the bluff body, one on either side of it. Figure 26 shows the test stand setup with one of the three bluff bodies installed on it.

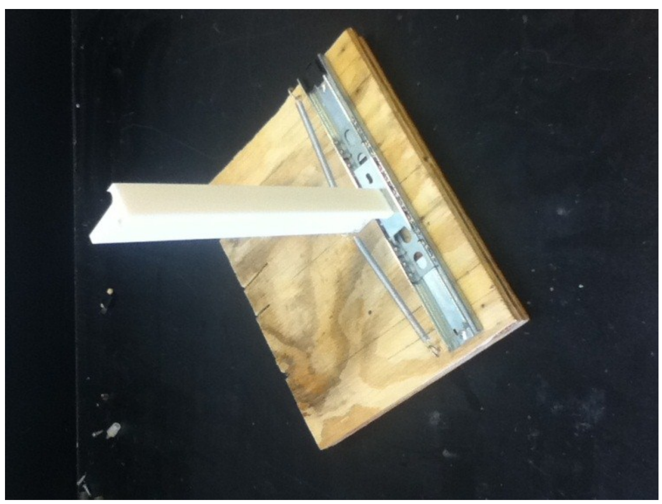

Figure 26: The Oscillating Test Stand Assembly

The test stand was secured on the bottom of the channel using a 10 lb weight, with the front face of the sliding rail being 2' 1½" from the front face of the channel. Figure 27 illustrates the proper setup of the test tank with the test stand in the channel. This figure also shows the test equipment in position to record displacement of the oscillating body.

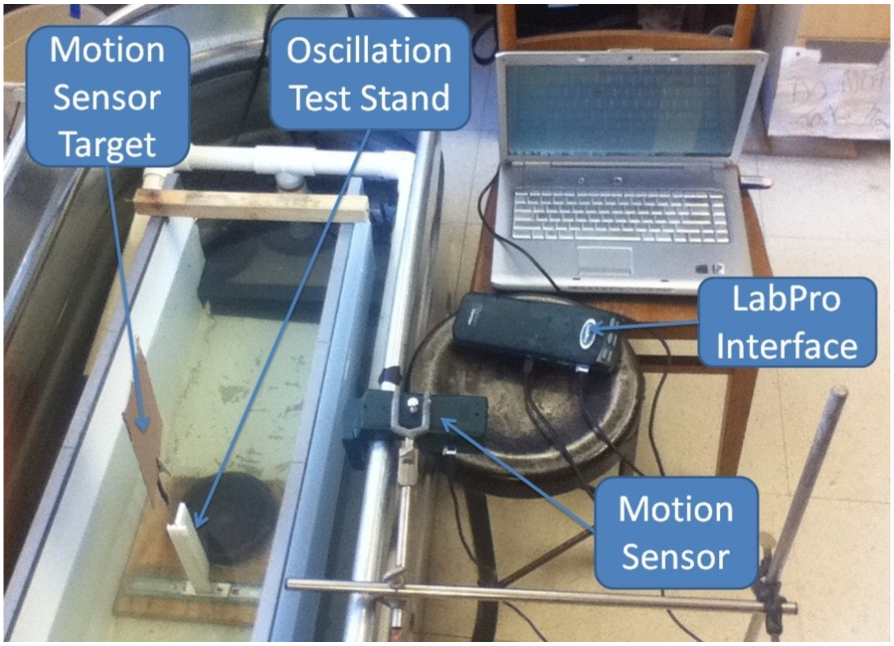


Figure 27: Motion Detection Test Setup Picture

After securing the test stand, the oscillation testing equipment was put in place. The motion sensor was plugged into interface input labeled DIG/SONIC 1 and the software automatically showed the displacement and velocity graphs for an object placed in front of the motion sensor. The motion sensor face was folded out and placed just over the edge of the test tank. The sampling rate was set to 20 samples per second; however any sampling rate between 15 and 25 samples per second proved to record data sufficiently.

Once the testing equipment was set up, the desired pumps were turned on. The team allowed the water to move about the channel for a few minutes to decrease any chance for disturbances resulting from initiating the fluid flow. The team then assured the test piece was oscillating properly. When the flow became fairly consistent, data was recorded utilizing the LoggerPro equipment. Figure 28 shows the testing in action. A button with a green arrow labeled “Collect” within the software initiates data collection. Each trial ran for 1 minute, with a total of 3 trials per test configuration. The same button used to initiate data collection switched to a red square labeled "Stop," which is then used to end data collection.  The test data was named accordingly for each trial and saved to the computer.

Figure 28:  Oscillation Measurement (Action Shot)

This process was completed for the three pump configurations (velocities 1, 2, and 3) for the first shape.  The test stand was then broken down, the next shape was installed, everything reassembled and testing of the second shape was performed.  The process was then repeated a third time for the third shape.  All data from the different tests were saved in separate folders to avoid confusion.

# 5. Results and Analysis

## 5.1 Fluent FEA Trials for Basic Shapes

In order to find which general shape would create the highest lift force, FEA tests were first conducted for some basic shapes using Ansys 12 Fluent tests. As stated previously, these tests were done using a 2 dimensional geometry in the X and Y directions of the coordinate system and assumed infinite length in the Z direction. The boundaries of the flow field were 20 times the characteristic length high by 30 times the characteristic length wide. The shape was positioned at 10 times the characteristic length down from the top, and 10 times the characteristic length to the right of the inlet. The tests were conducted using the following Reynold's numbers: 100, 150, 200, 500, 1000, 2000, 3000, 4000, and 5000. The characteristic length of the shape (i.e. diameter) was kept constant at one meter, and the density property of fluid was varied to achieve the desired Reynold's number. The flow was set at transient flow with a constant dynamic viscosity of 1 $N*s/m^2$ and a constant velocity of 1 m/s. The basic shapes tested can be viewed in Figure 29, and include a square, rectangle, triangle, and ellipse. The triangle went through two rounds of testing: one round with the point into the flow, and one with point away from the flow. The ellipse went through two round of testing as well: one with the semi-major axis perpendicular with the flow, and one with the semi-major axis perpendicular to the flow. The T-shape was tested with the flat top into the flow.

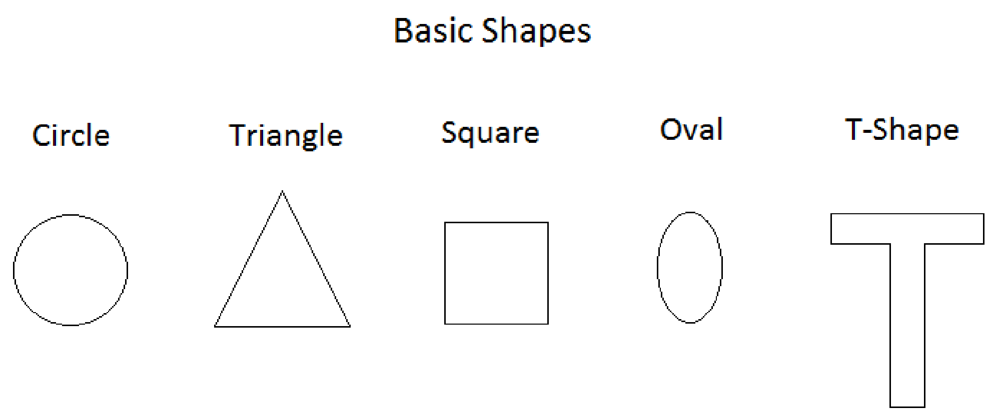


Figure 29: Overview of Basic Shapes

The first shape tested was the triangle. The first triangle test was conducted with the point of the triangle into the flow. The lift coefficient at low Reynold's numbers was 0.0001, and was 0.01 at higher Reynold's numbers. The second triangle test was conducted with the point facing away from the flow. The resulting lift coefficient was much better than the previous way the triangle was tested. At low Reynold's numbers the lift coefficient was around 0.08, while at higher Reynold's numbers the lift coefficient was about 1.4. This test clearly shows the triangle has higher performance with tip facing away from the flow, instead of into the flow as previously suggested by background research. The lift coefficient graph as well as the vorticity and pressure charts for the triangle can be viewed in Figure 30.

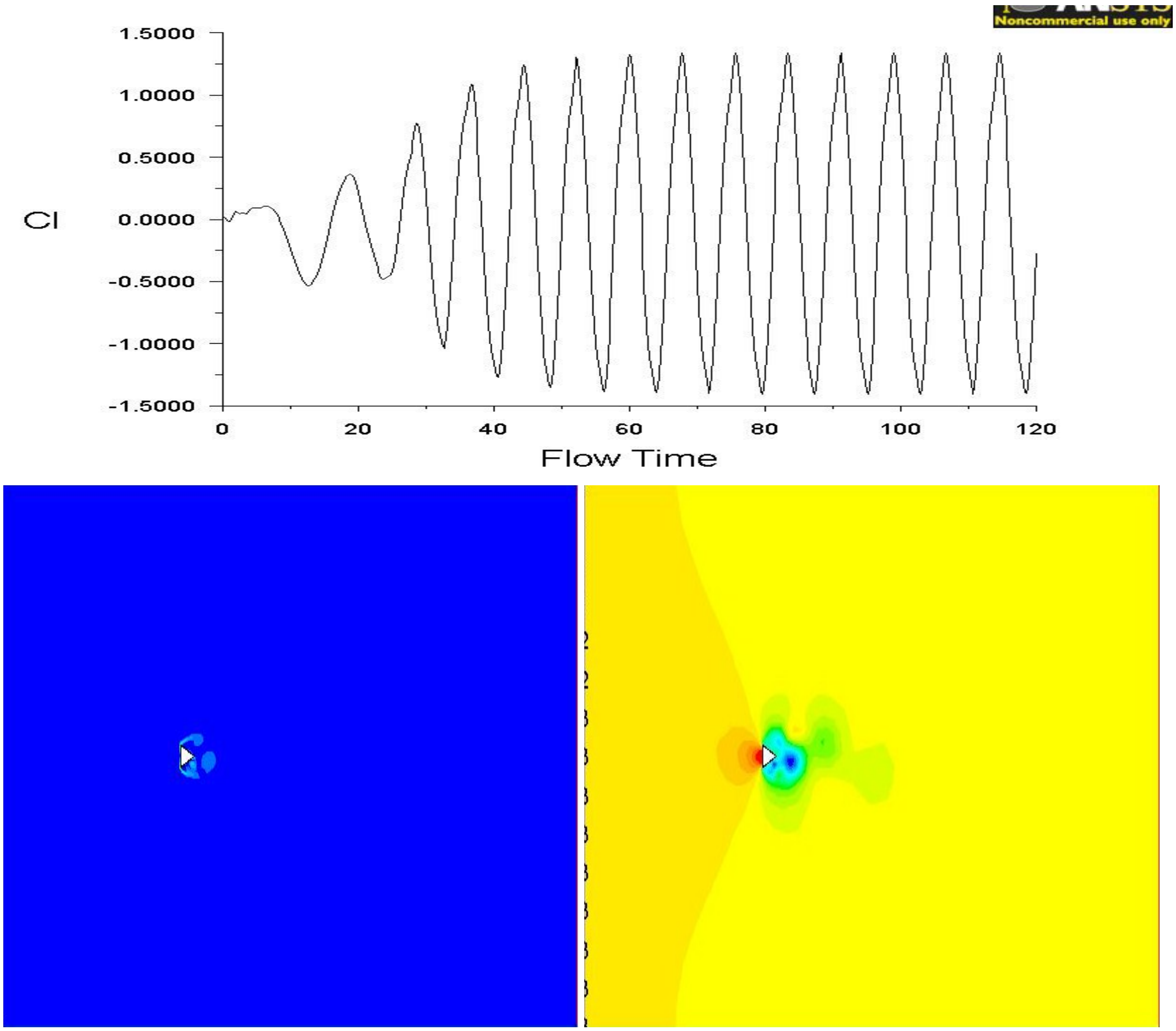


Figure 30: Front Triangle Fluent Results

The next shape tested was a simple square. At lower Reynold's numbers the lift coefficient was 0.005, and at higher Reynold's numbers the lift coefficient was 0.4. The square was found to have a lower lift coefficient than the triangle. There was also an issue with obtaining a stable oscillation in which after approximately 60 seconds, the shape would no longer generate lift, perhaps indicating this shape is not geometrically able to produce sustainable vortices. This phenomenon is shown in the lift coefficient graph, which can be viewed along with vorticity and pressure charts for the square in Figure 31.

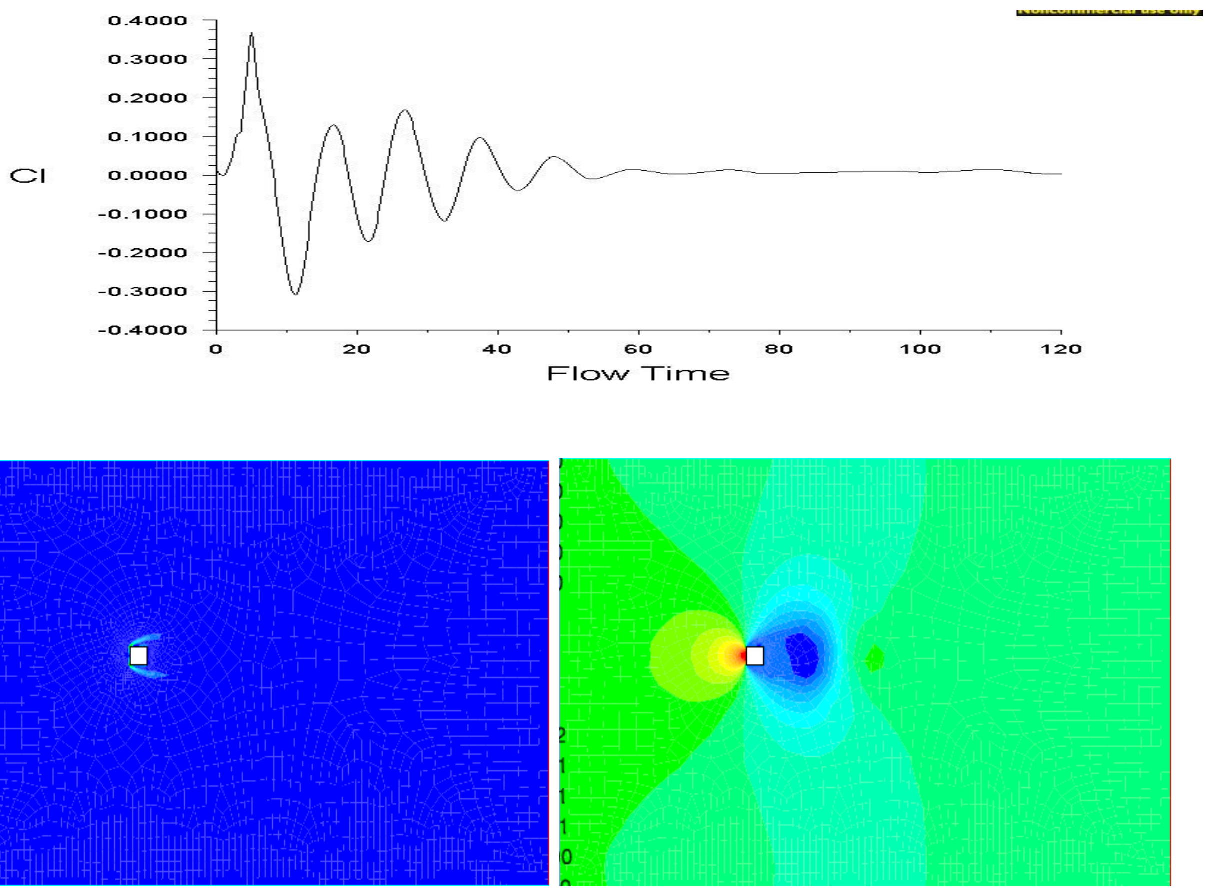


Figure 31: Square Fluent Results

The next shape tested was the ellipse. The first test included an ellipse with length to width ratio (L/W) of one quarter.  At lower Reynolds's numbers, the lift coefficient was found to be 0.02, and at higher Reynolds's numbers was found to be 0.1. The ellipse also experienced the same phenomenon as the square, in which it would no longer produce lift forces after 60 seconds. The second test included an ellipse with an L/W of two.  At lower Reynolds's numbers the lift coefficient was found to be 0.035, and at higher Reynolds's numbers, the shape failed to produce oscillating lift coefficients. Due to the inability of the ellipse to generate oscillating lift coefficients, this shape is not recommended for the use of generating vortices. The lift coefficient graph as well as the vorticity and pressure charts for the ellipse can be viewed in Figures 32 and 33.

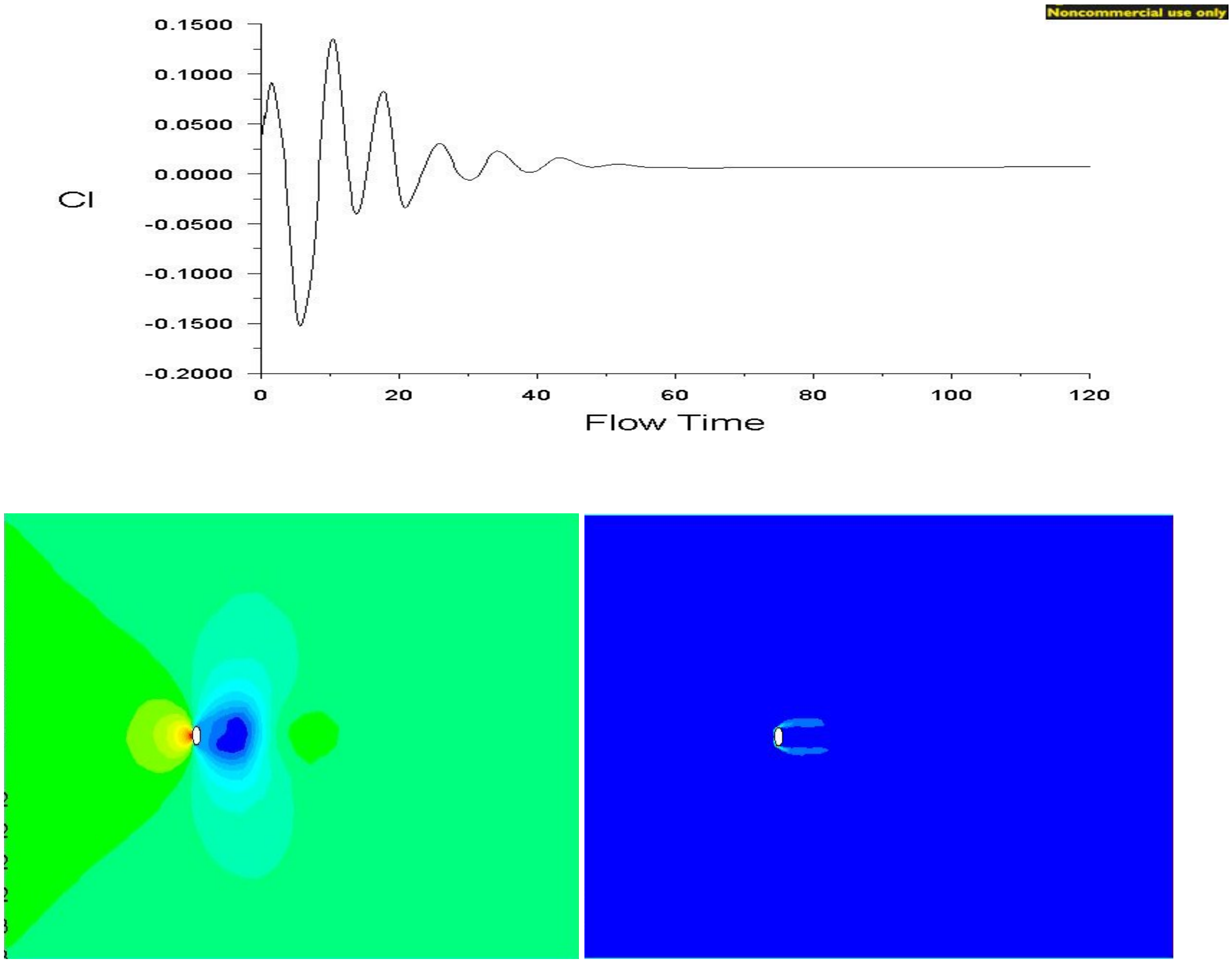


Figure 32: Ellipse L/W = 0.25 Fluent Results

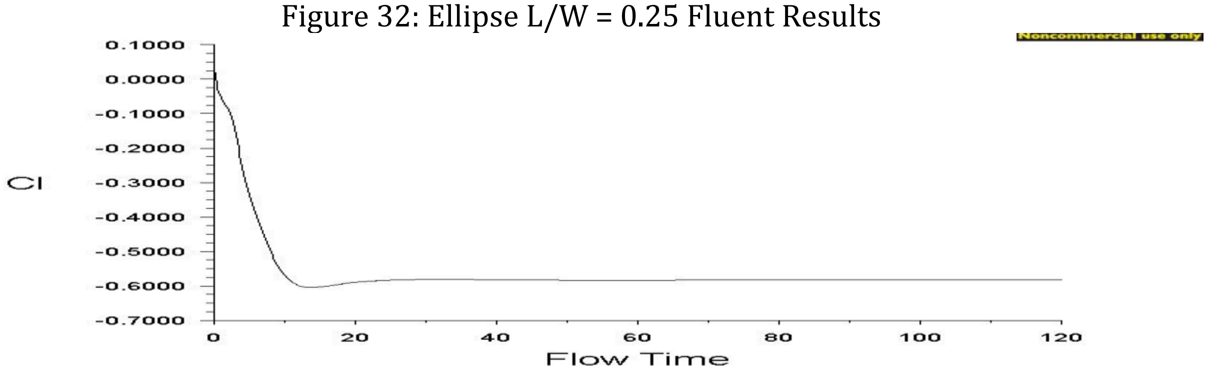

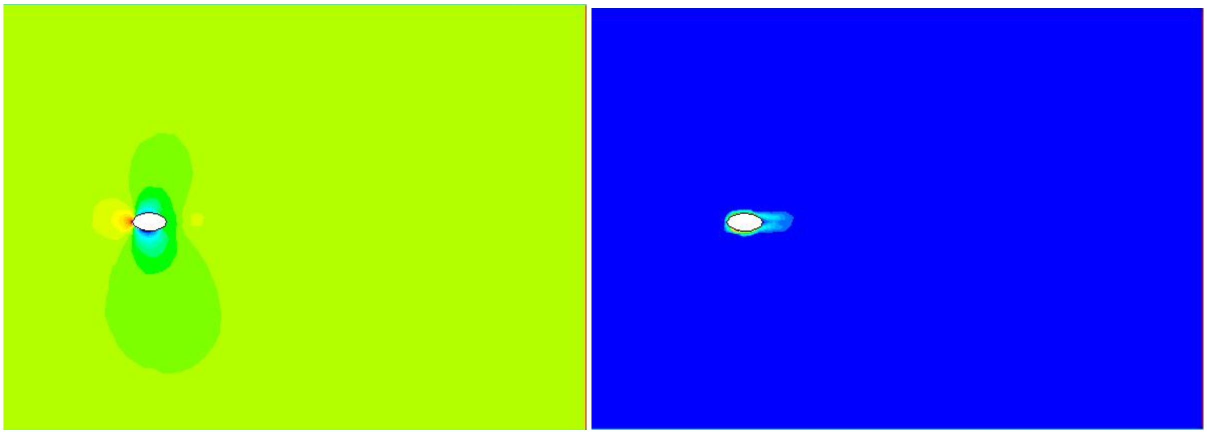

Figure 33: Ellipse L/W = 2 Fluent Results

The second to last shape tested was the cylinder. At low Reynold's numbers, the circle produced a lift coefficient of .25, and at high Reynolds numbers produced a lift coefficient of .45. This shape produced an interesting lift coefficient graph as the amplitude of the coefficient seemed to be random and sporadic. This indicates the shape would not be able to output consistent displacement amplitude during the physical testing. The lift coefficient graph, vorticity chart, and pressure chart can be viewed in Figure 34.

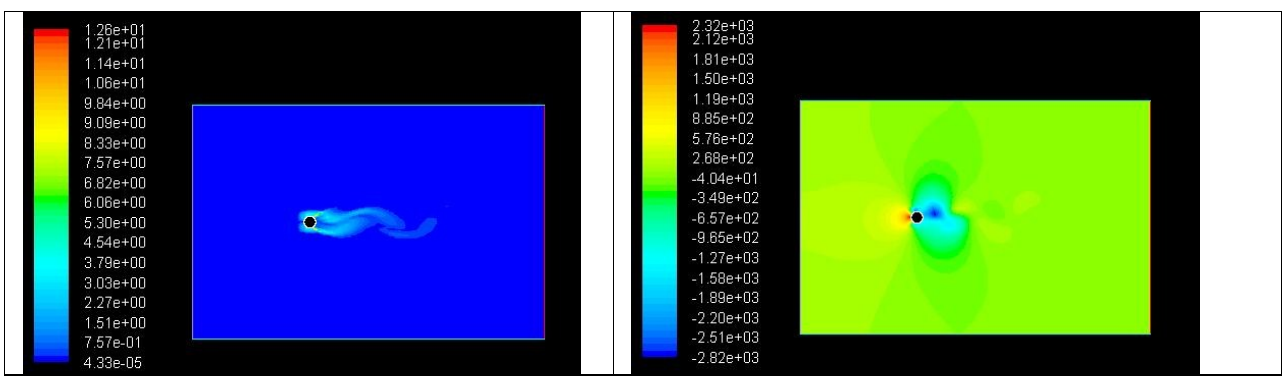

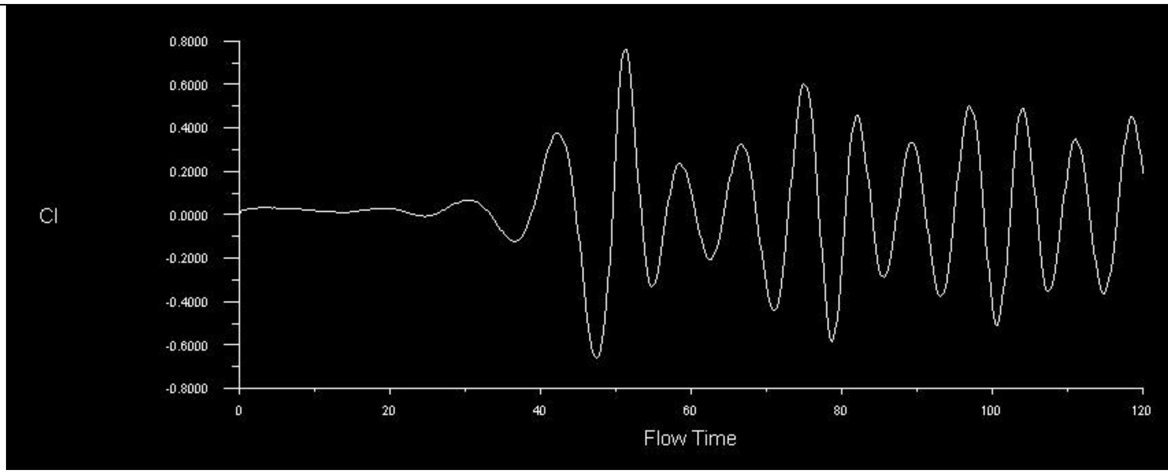

Figure 34: Circle Fluent Results

The final shape tested was the T-shape. This shape produced a lift coefficient of .17 at low Reynold's numbers and a lift coefficient of 1.8 at high Reynold's numbers. This shape produced the largest lift coefficients out of all the other basic shapes, and was selected to determine which shape variation would produce the largest lift coefficient. One possible theory about why the T-shape produced the largest amplitudes was that it had a flat face into the flow, and the horizontal piece of the T (as viewed in Figure 37) acted as a splitter plate allowing the force of the pressure difference to act on the shape for a longer period of time. The lift coefficient graph as well as the vorticity and pressure charts for the T-shape can be viewed in Figure 37.

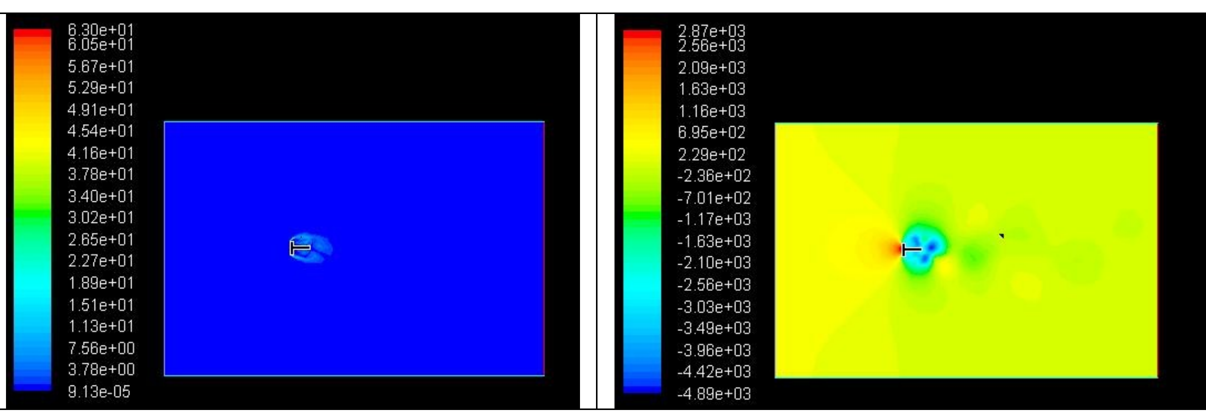

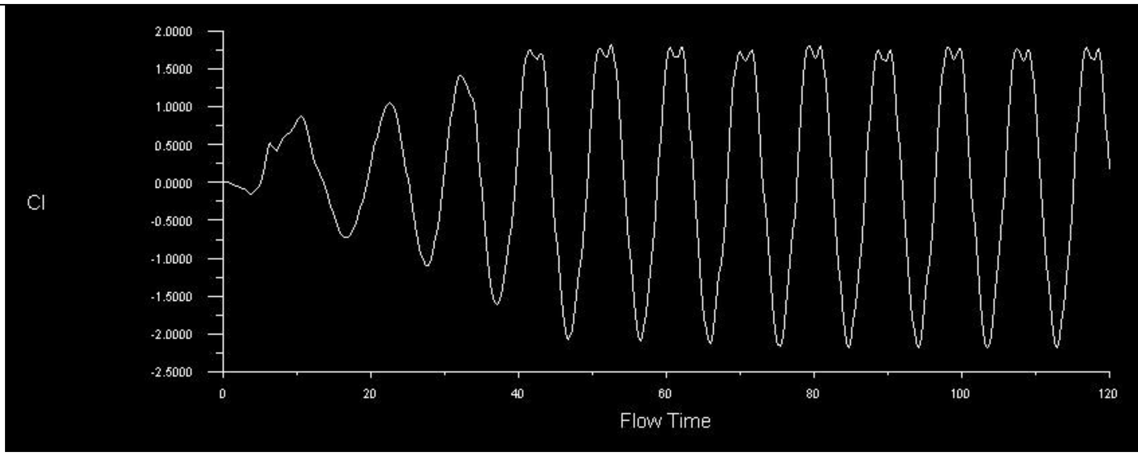

Figure 35: T-Shape Fluent Results

Figure 36 shows the summarized results for the lift coefficients of the basic shapes that were tested in Ansys Fluent. As can be seen by the graph, a shape with a front facing, flat edge out performs all the other basic shapes. One possible reason for this is that having sharp edges on the side facing the flow creates a greater pressure differentiation which aids in the development of stronger vortices. The results show that the T-shape generates the highest lift coefficient, followed closely by the triangle with the tip facing away from the flow. The ellipses, square, and triangle facing into the flow show minimal lift coefficients and were concluded to not perform well in physical tests. The T-shape was selected to continue to the next round of testing because of its indication it would produce the largest amplitudes in the physical trials since it generated the largest lift coefficients.

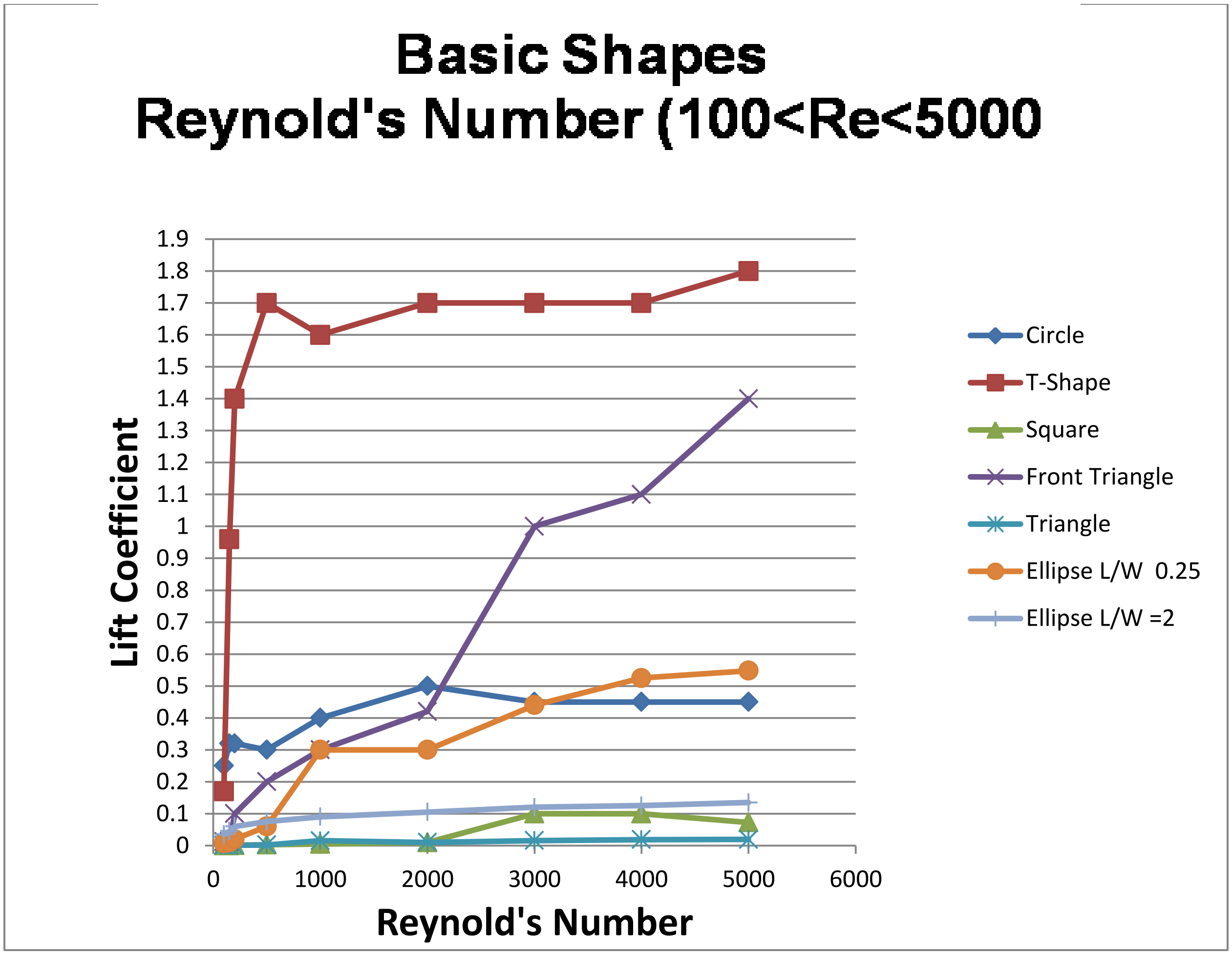


Figure 36: Summarized Results of Basic Shapes from Fluent Testing

### 5.2 T-Shape Trials

After concluding the T-shape cylinder would produce the most lift out of the common shapes, variations of the T-shape were tested in order to optimize the cross sectional shape. These shapes include a circular T-shape, a triangular T-shape, a Y T-shape, a parachute T-shape, a double-Y T-shape, and concave T-shape. These shapes can be observed in Figure 37. As with the basic T-shape, all varied T-shapes were orientated with the T part facing into the flow. A low Reynold's number of 150 was compared with a high Reynolds number of 5000.

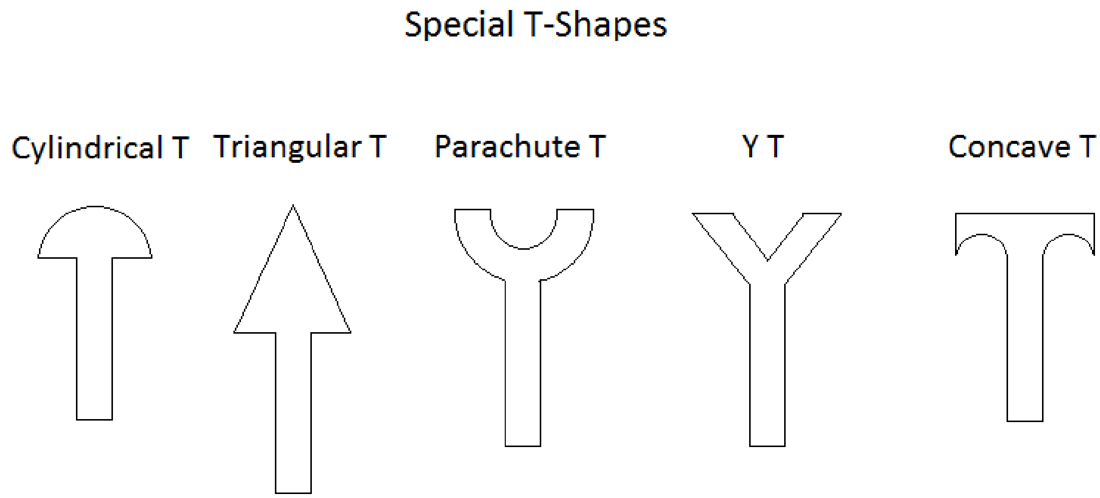


Figure 37: T-Shapes

The first shape that was tested was the Cylindrical T. At low Reynold's numbers, the cylinder produced a lift coefficient of .11 and at high Reynold's numbers produced a lift coefficient of 1.15. This is considerably less than the lift coefficient of the t-shape and indicates it would not produce large amplitudes during physical testing.

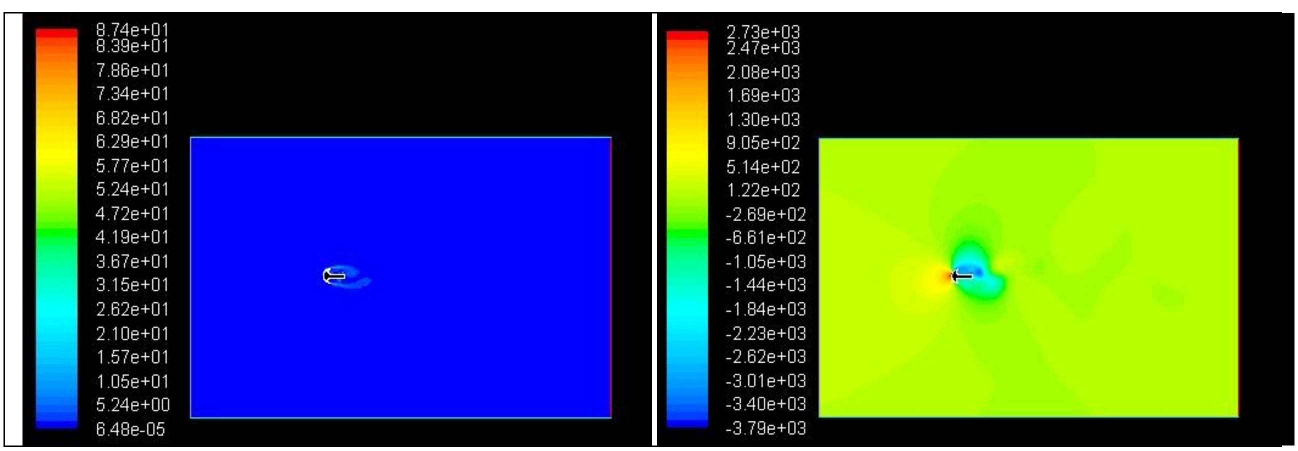

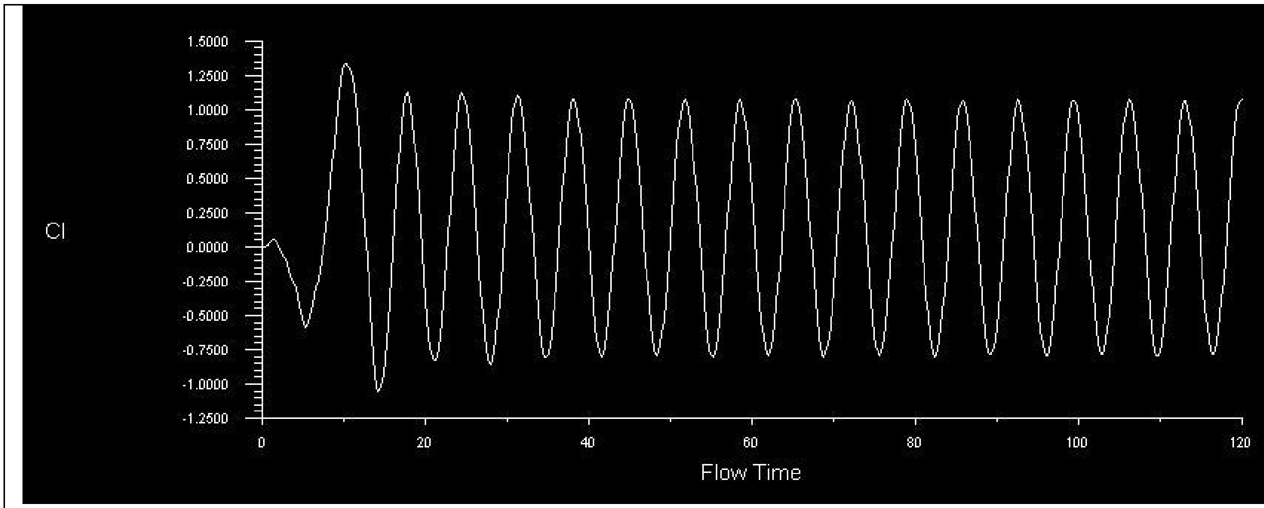

Figure 38: Cylindrical T-Shape Fluent Results

The Triangle-T was tested next. It produced a lift coefficient of .01 at low Reynold's numbers and a lift coefficient of .85 at high Reynold's numbers. Again, this lift coefficient was much lower than the original T-shape.

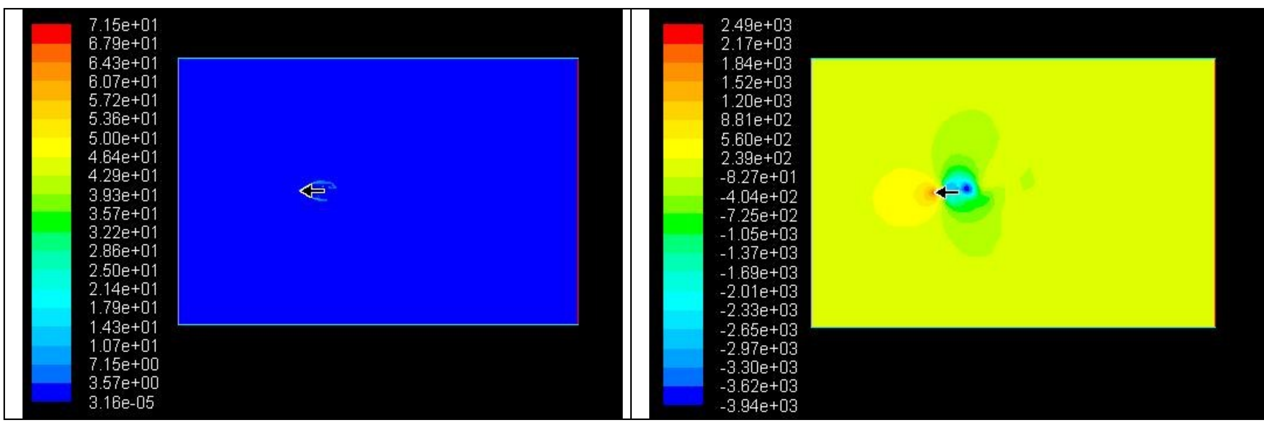

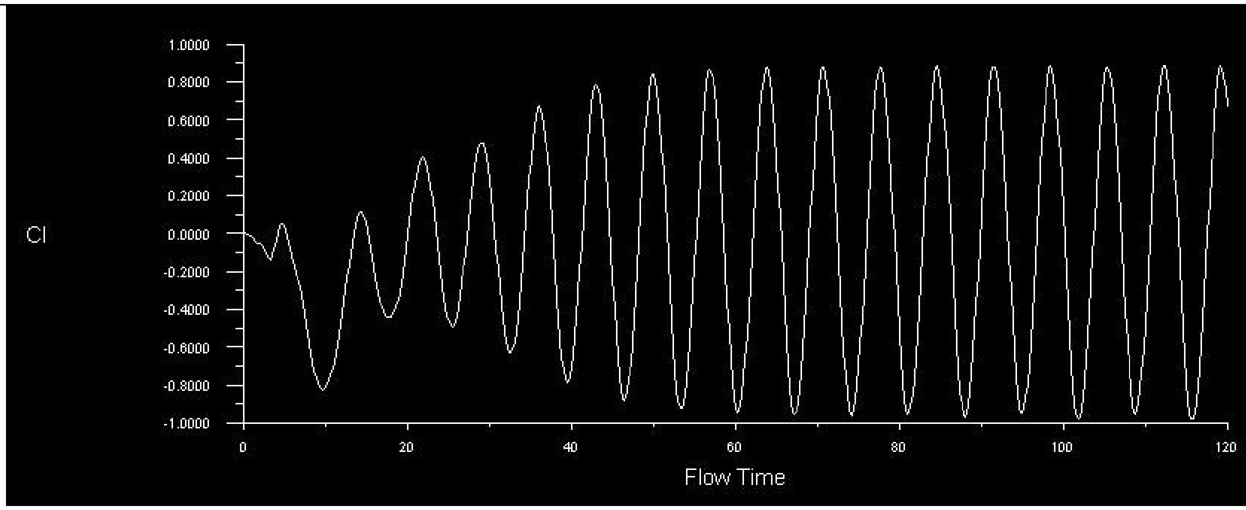


Figure 39: Triangle T-Shape Fluent Results

The Y T-shape was tested and was found to have a lift coefficient of 1.65 at lower Reynold's and a lift coefficient of 2 at higher Reynold's number. These lift coefficients indicate this shape would perform better than the original T-shape.

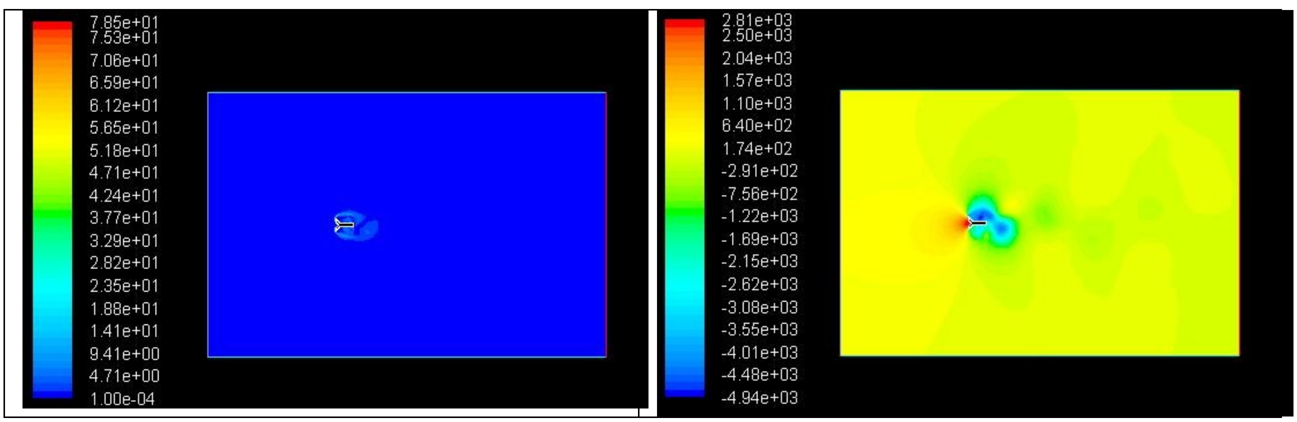

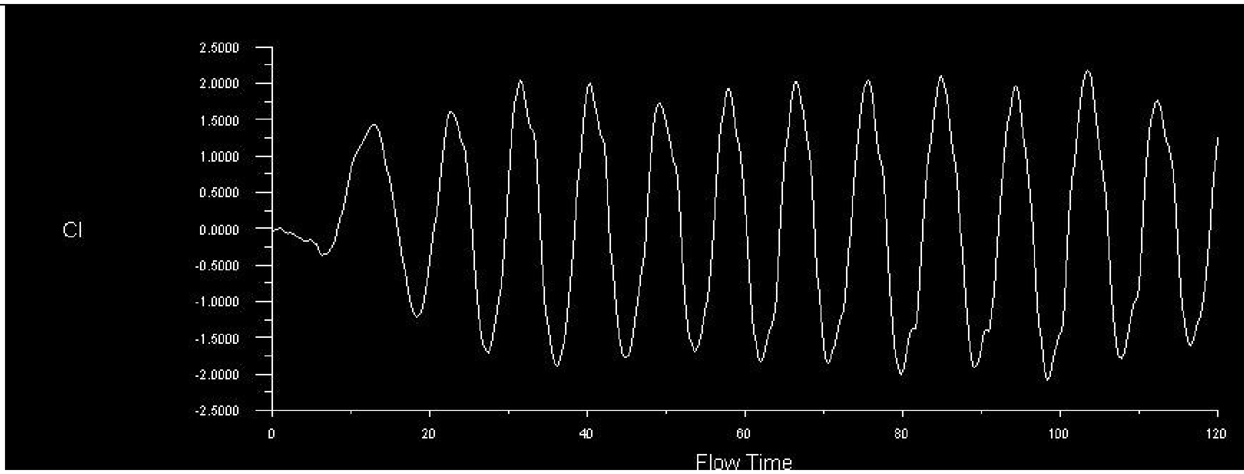


Figure 40: Y-T-Shape Fluent Results

The parachute shape was test and was found to produce a lift coefficient of .4 at lower Reynold's numbers and a lift coefficient of 1.9. These lift coefficients indicate this shape would perform better than the original T-shape.

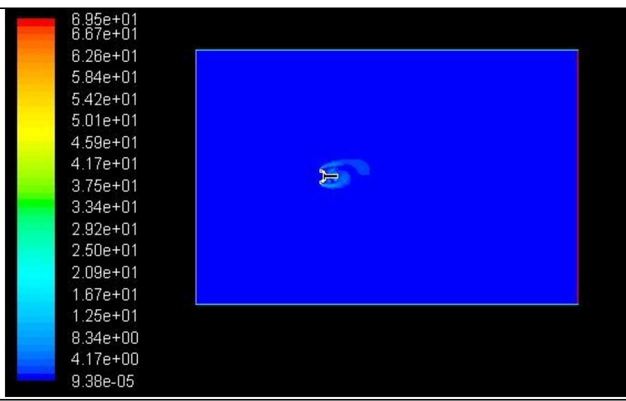


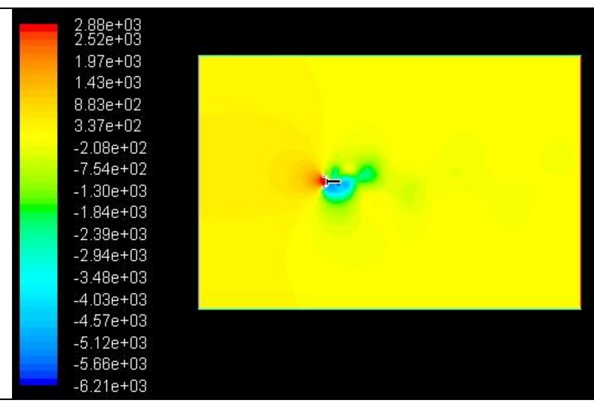

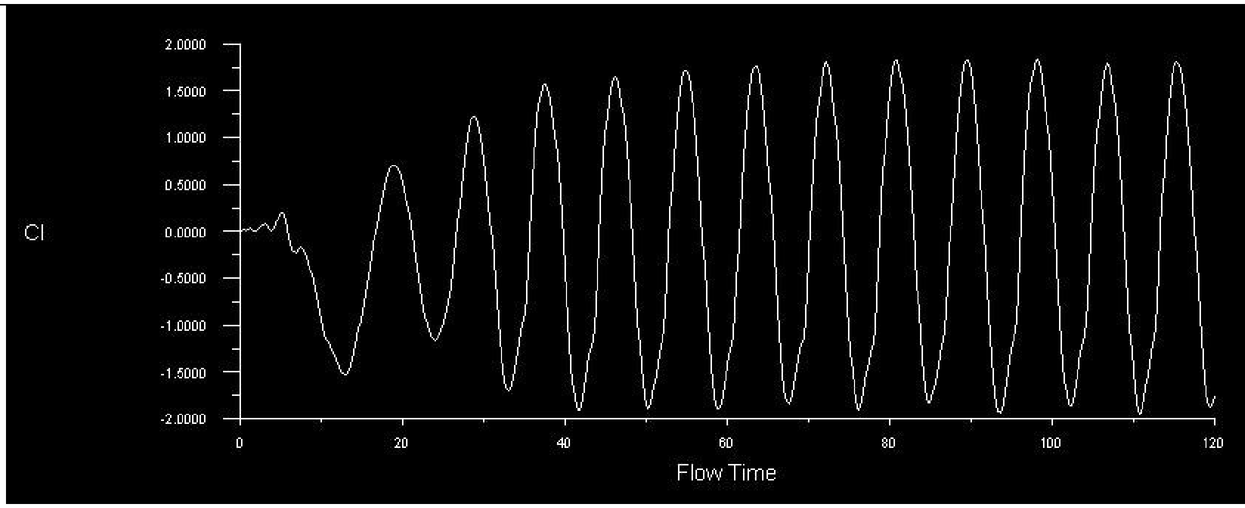


Figure 41: Parachute T-Shape Fluent Results

The last shape to be tested was the Concave-T shape which produced a lift coefficient of .01 at low Reynold's numbers and a lift coefficient of 2.2 at high Reynold's numbers. These lift coefficients suggest that this shape will perform better than the original T-shape.

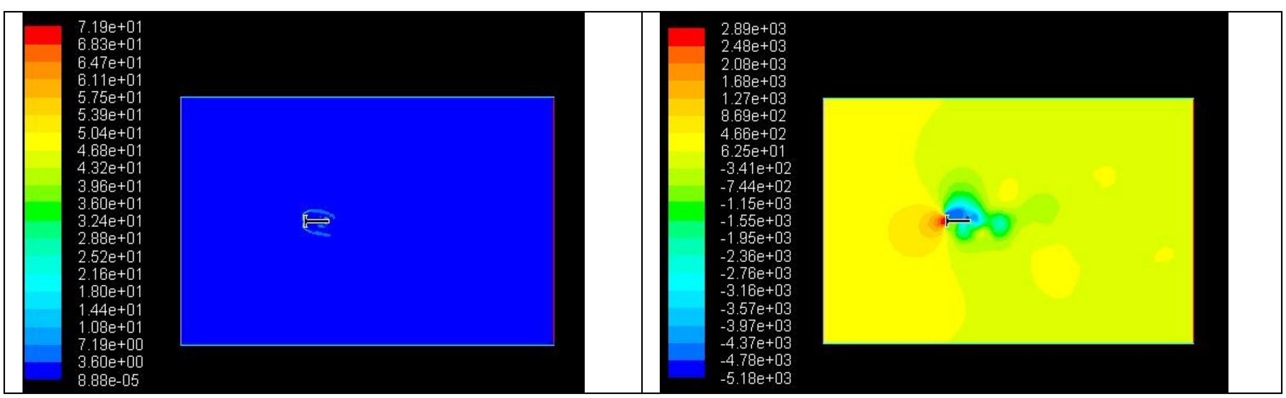

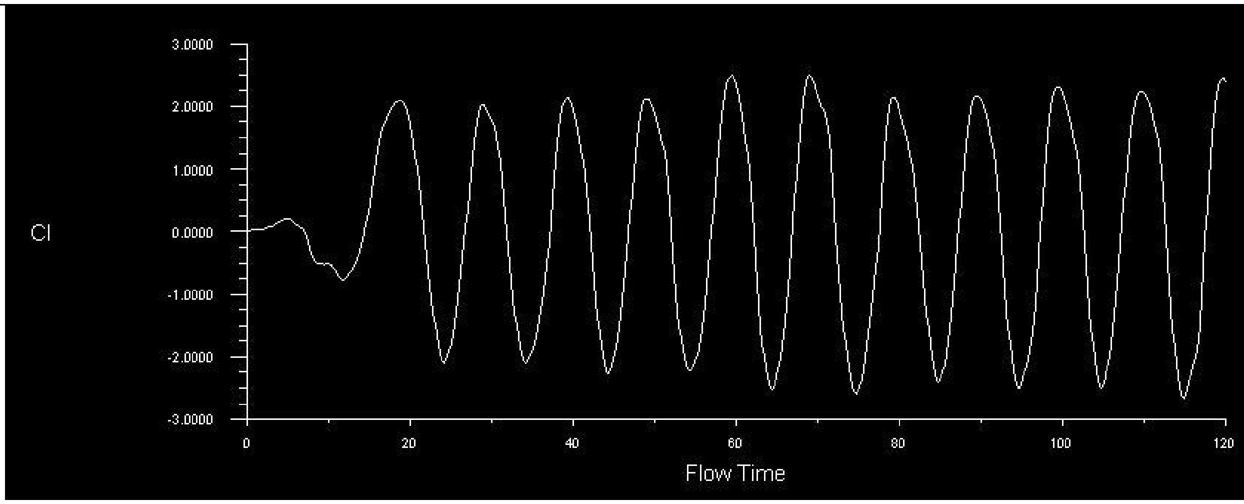

Figure 42: Concave T-Shape Fluent Results

Figure 42 shows a summary of the T-Shapes performance over a range of Reynolds numbers. From this graph it is obvious that the Concave-T shape had the highest performance in terms of the lift coefficient and the cylinder had the lowest performance. Other shapes that performed well were the Parachute-T shape, the Y-T shape and regular T-shape.

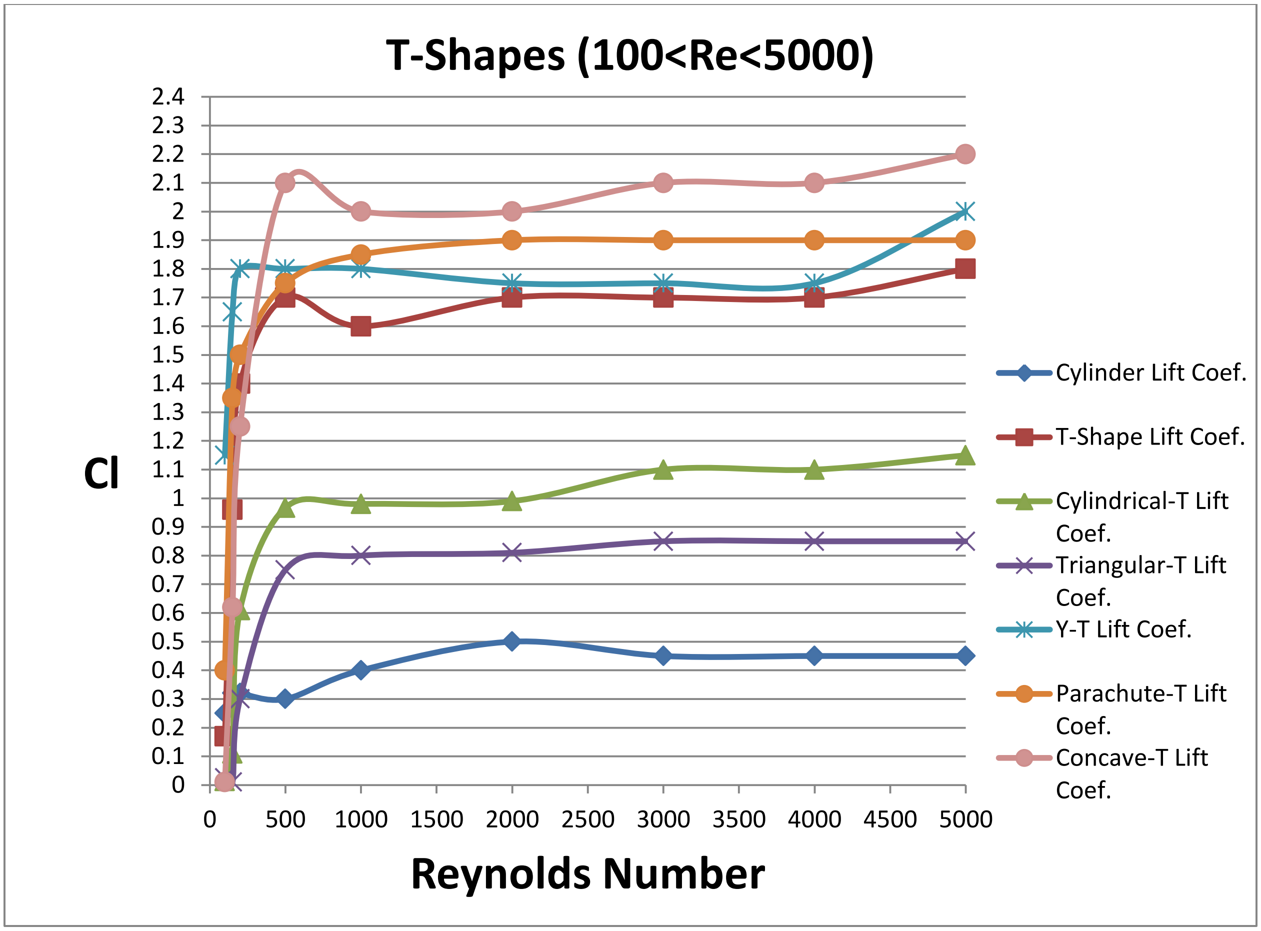


Figure 43: Summary of T-Shape Fluent Testing

Figure 43 shows various T-shapes tested at higher Reynolds numbers. The purpose of these tests was to examine the top four shapes at higher Reynolds numbers and determine their performance. The Concave-T shape again had the best overall performance and held a constant lift coefficient of 2.4. The Y-T shape started with the highest lift coefficient of 2.6 but sharply declined in higher Reynolds numbers down to 2.2. The T-shape and Parachute-T shape held relative stable lift coefficients of approximately 1.8.

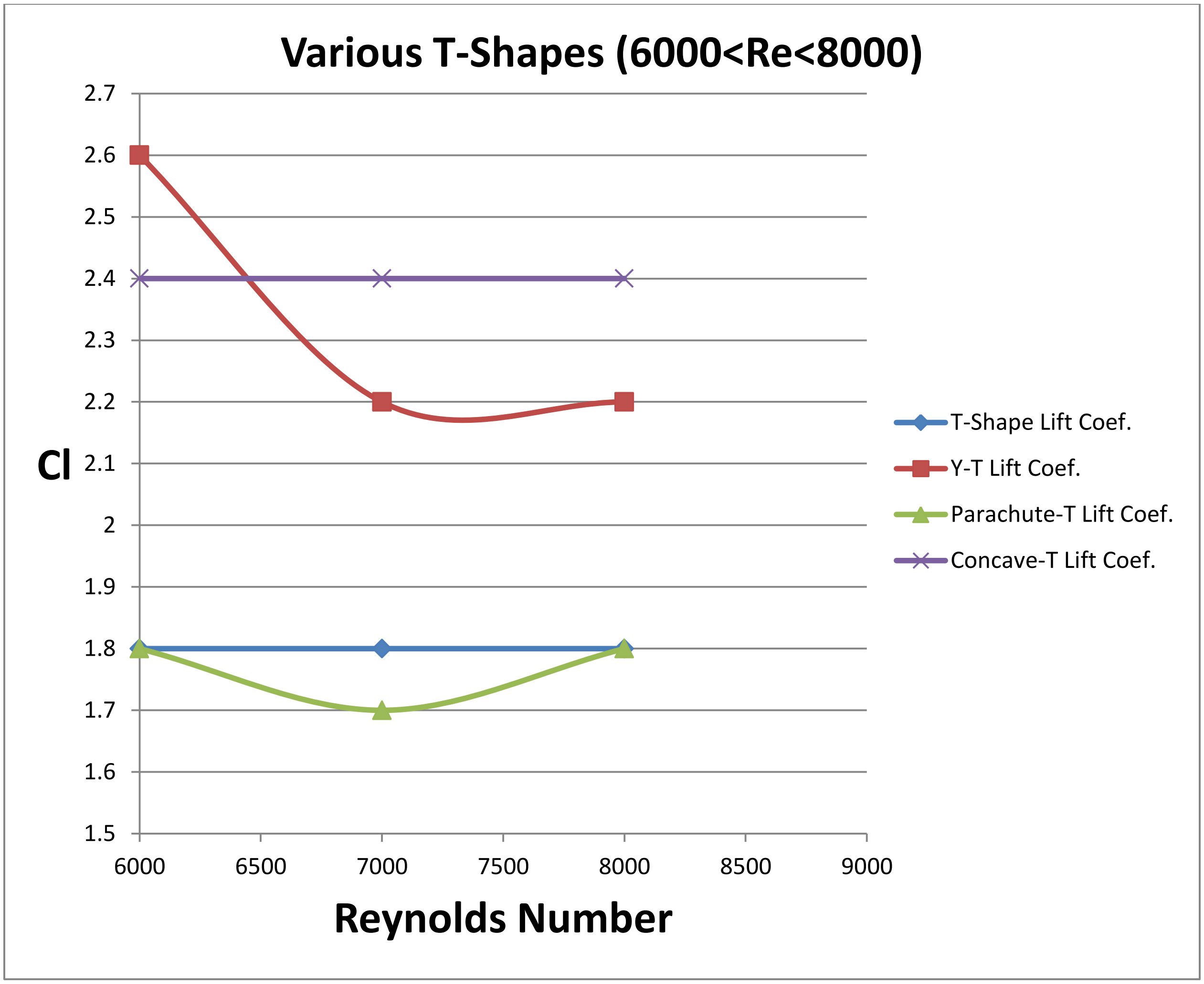


Figure 44: Summary of Four Best Performing T-Shapes at Higher Reynold's Numbers

Figure 45 shows how various T-shapes might react under estimated operating conditions. Given an estimated characteristic length of six inches, and flow velocity of about 2 knots, the resulting Reynolds number was 140,000. At this Reynolds number, the Concave-T had the best performance with a lift coefficient of 2.1. Both the Y-T shape and the Parachute-T shape had the lowest performances with lift coefficients of 1.4 and 1.2, respectively. The T-shape had an average performance with a lift coefficient of 1.8. The Concave-T shape consistently performed the best out of all of the shapes, and thus was selected for manufacturing and physical test tank trials. One of the reasons the Y and Parachute-T shapes had lower performances at higher Reynolds numbers may be because the fluid in frontal area of the shape became stagnant and was unable to flow around the shapes due to the higher pressures. This would create a pressure bubble which would make the shapes perform similar to the Circular-T.

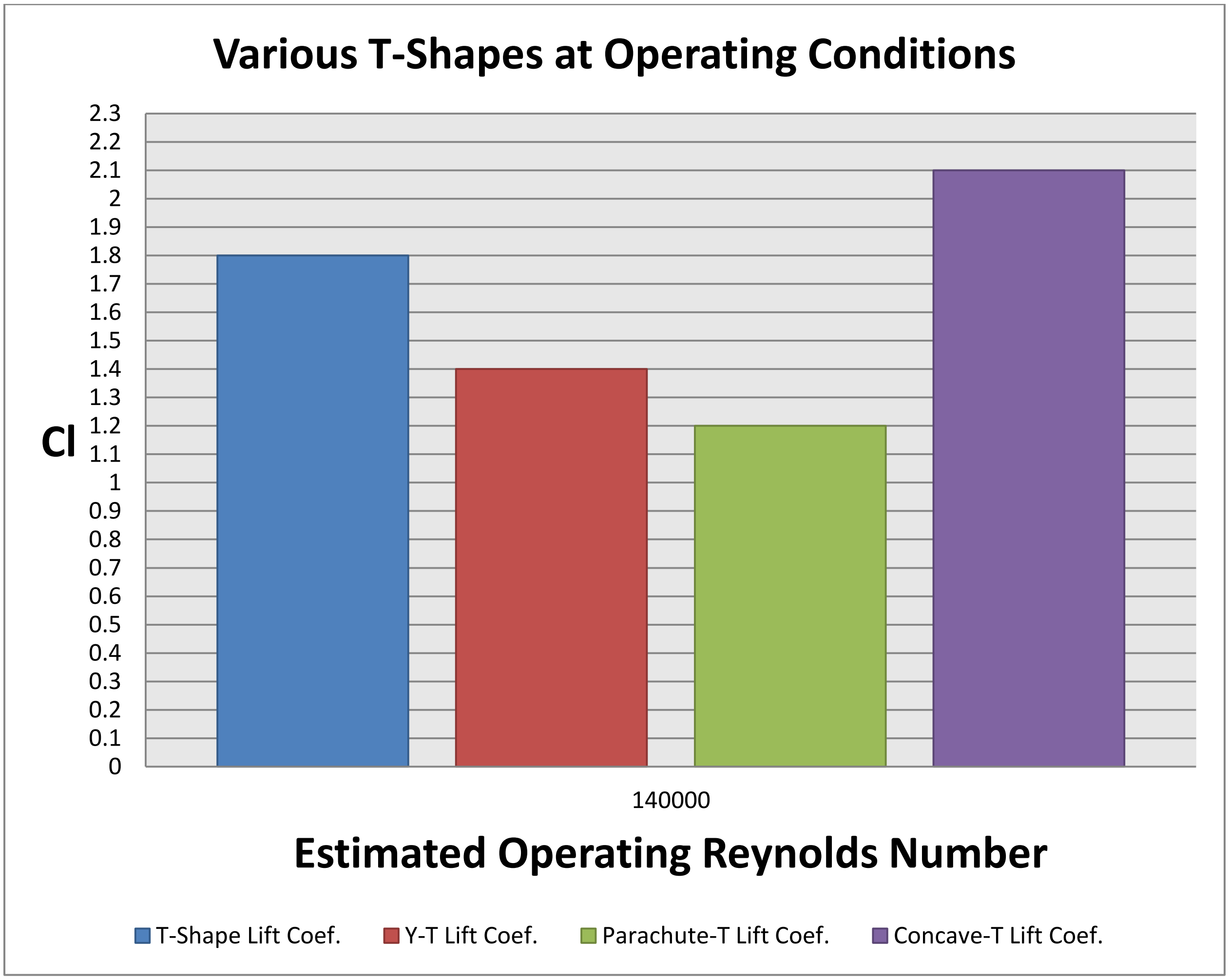


Figure 45: Various T-Shapes at Operating Conditions

## 5.3 Flow Velocity Testing Results

The 3 separate 1-minute trials were averaged together… and averages for each individual point as well as for each individual pump configuration are shown in the table in Appendix F.  The data were farther simplified into Table 2 shown, which provides the average flow velocity for all 11 points. However, since the shape will oscillate primarily in the center of the test channel and not too often near the test channel walls, a second average was taken. The center average flow velocity averages the values for the velocity of points TL2, TMID, TR2, CENTER, BL2, BMID, and BR2 (these point's locations are shown in Figure 24 on page 54. The center averages will be slightly higher due to frictional resistance of the water flowing near the walls of the test channel.

| **Pump Horsepower In Use** | **Average Flow Velocity** | | **Center Average Flow Velocity** | |
|---|---|---|---|---|
| | meters/second | inches/second | meters/second | inches/second |
| 1/3 | 0.15 | 5.8 | 0.19 | 7.4 |
| 1/2 | 0.26 | 10.4 | 0.30 | 11.9 |
| 5/6 | 0.34 | 13.6 | 0.39 | 15.2 |

Table 2: Average Flow Velocities for Different Pumps in Use

To better show the velocities at each point, a line with a length that corresponds to the velocity at each point was sketched in the direction of the flow, with the beginning of the point being at the point where the velocity was measured. The line's lengths (in inches) are equal to 10 times the velocity (in meters per second) at each of the points. To enable all lines to be seen at once, the views shown in the figures below are from the side of the test area, but slightly from above. The point at which the measurements were taken are in the center (left to right) of the segment of test channel shown. In these representations of the flow, the water is flowing from right to left. For reference, the length of the test section shown is 12 inches.

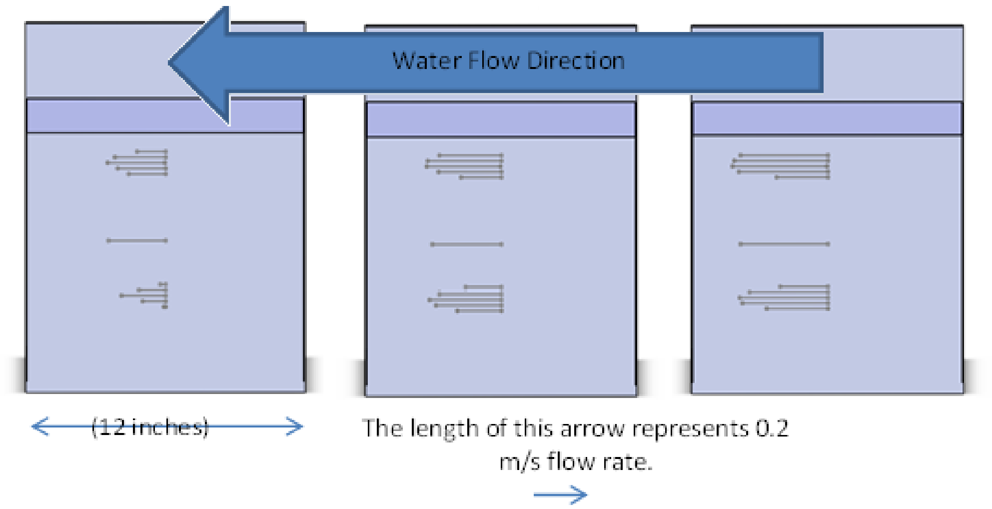


Figure 46: Velocity Profile Line Sketch of 1/3 hp pump (Left), 1/2 hp pump (center), and 5/6 hp pump (right)

Figure 47 is shown below to help visualize the profile in an isometric view. This figure shows the results for the 1/3 HP pump. In this figure it is much easier to visualize how a section of flow channel has been taken out for illustrative purposes. The plane shown indicates the plane at which the flow meter was located for all 11 points, which is also the plane that our test shape was located.

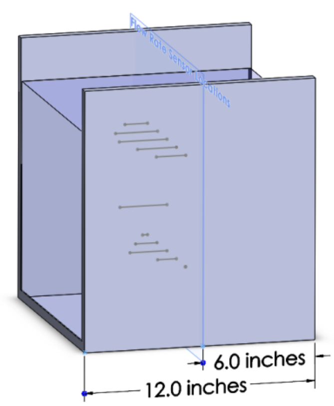


Figure 47: Velocity Profile Isometric View (1/3 HP)

## 5.4 Physical Testing Results

After the testing of the shapes was finished, the results could then be determined and conclusions could be determined. From the Logger Pro data we were able to record and analyze the displacement of the shape. The curve produced was a sine curve, meaning that the shape would move to one side and then back to the other side, with the zero point being right in the middle of the channel. From interpretation of the data, we were able to calculate an average displacement and plot that value versus the power of the pump.

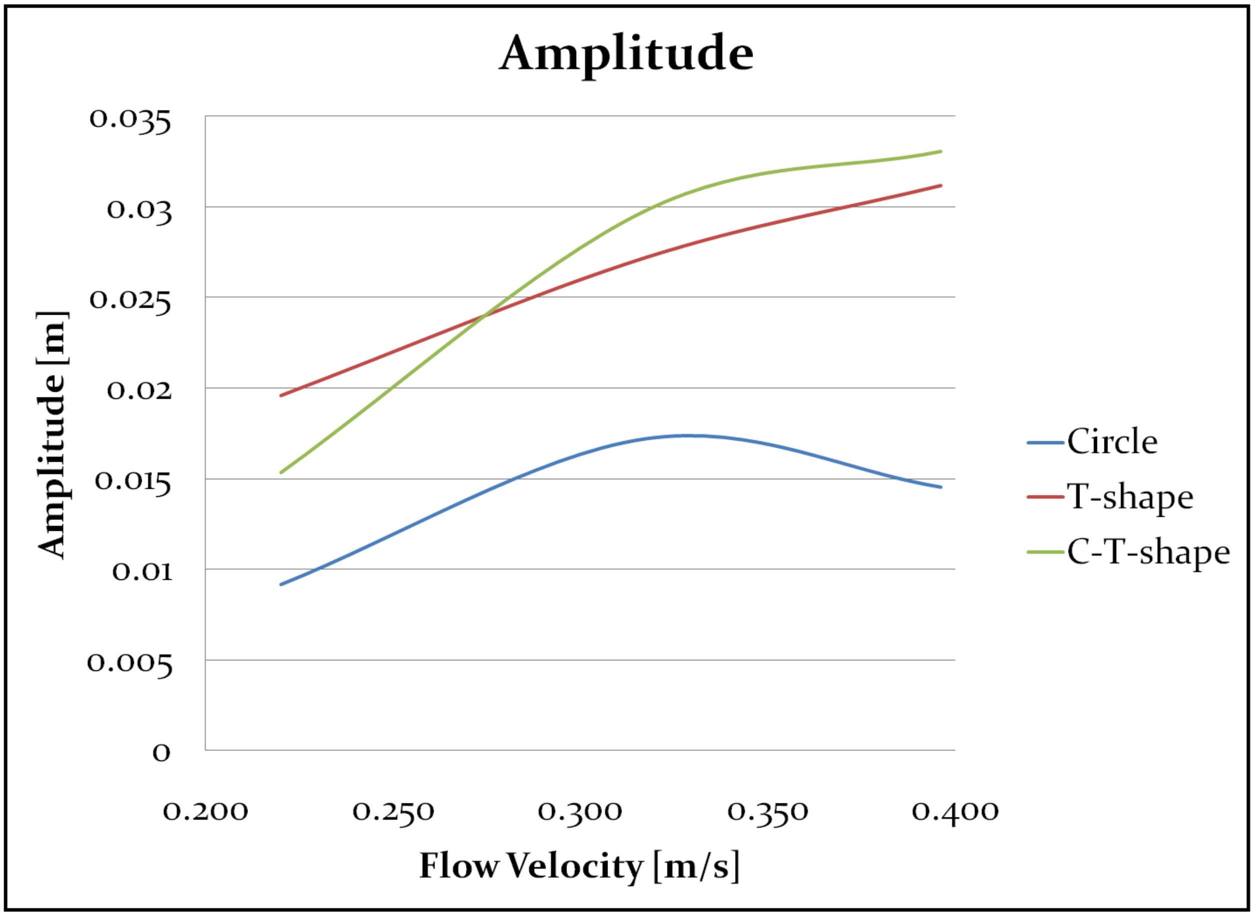


Figure 48: Amplitude Results from Physical Testing

There were three tests conducted at each speed, and the graph above shows the average displacement from each of the three test runs. As anticipated from the Fluent trials, the concave T-Shape produced the largest lift force and thus created the greatest amplitude.

Although the concaved T-shape produced the most amplitude, the circle produced the largest frequency.

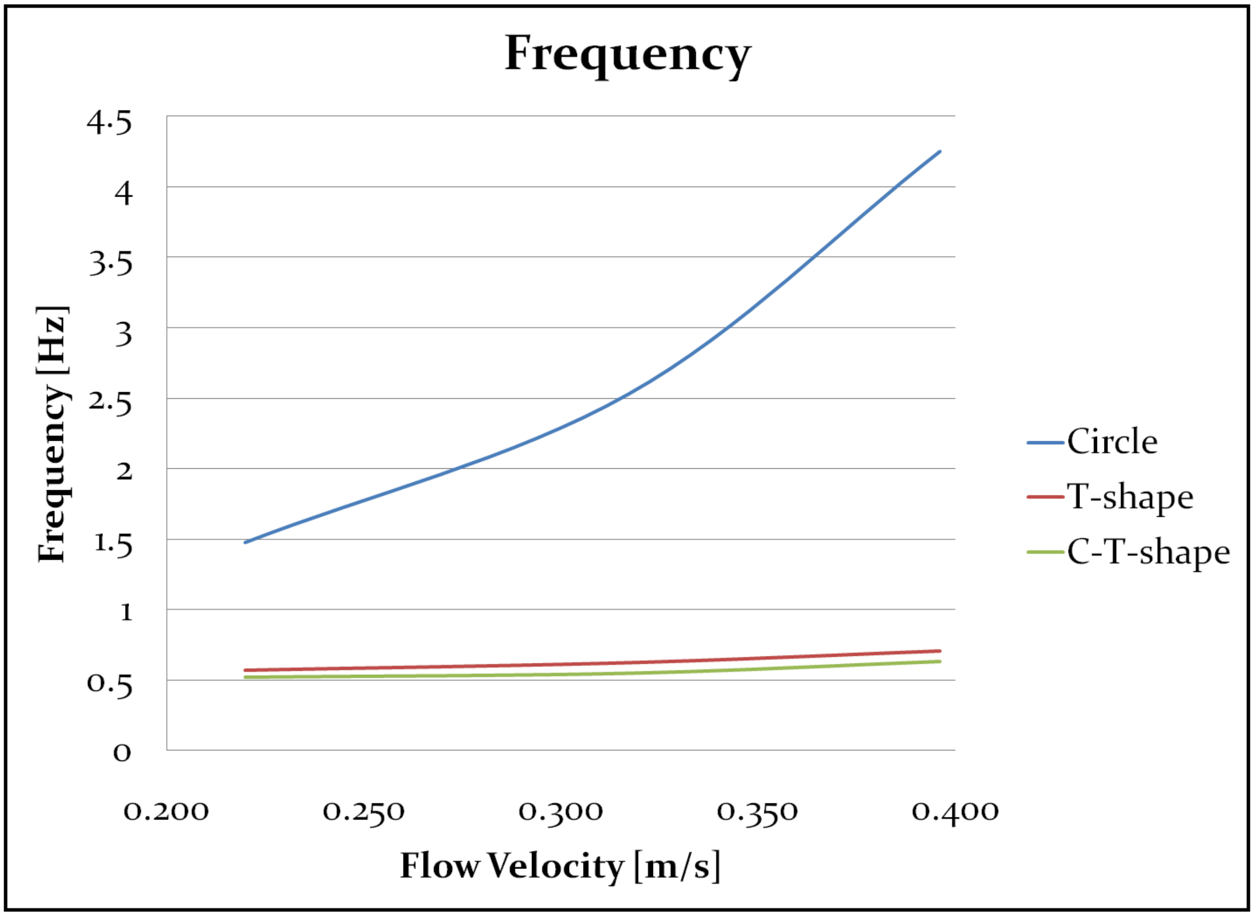


Figure 49: Frequency Results from Physical Testing

From Figure 49it can be seen that the frequency of the cylinder was 85% higher than the T-shapes. As a result the cylinder produced a higher mechanical energy in the system, because no torques were applied to the system.

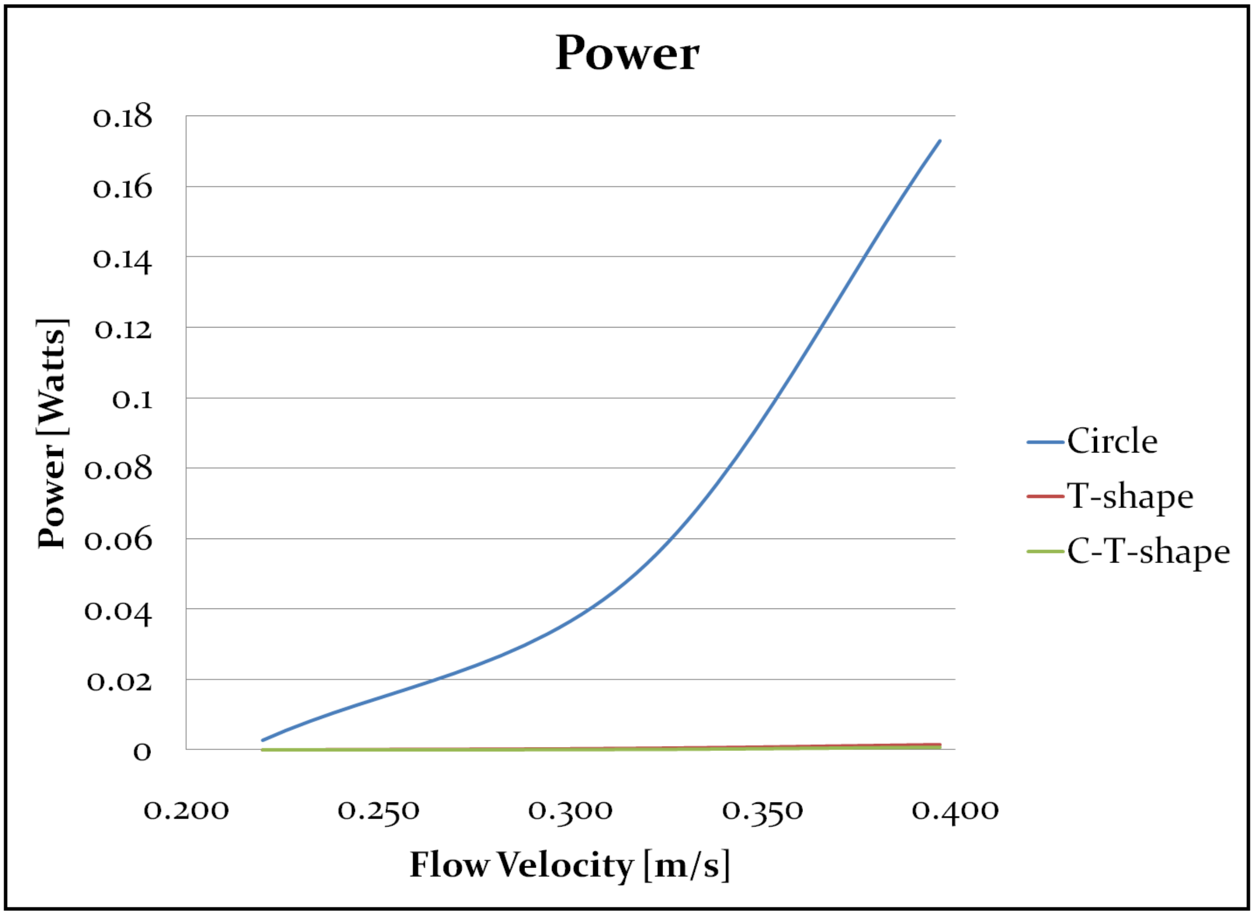


From Figure 49 the data collected the conclusions were made that for our current system constructed the cylinder would provide the most mechanical energy. This is a result of the frequency of the cylinder being the greatest. The power was calculated by first applying the root mean square to the initial sine wave curve for displacement. The root mean square is a statistical measure of the magnitude of a varying quantity. It can be calculated to avoid the negative displacement values, which were first obtained from the Logger Pro test data. Once the RMS was calculated the power could be calculated as a function of time using the following equation.

$$P(t) = v(t)(ma(t) + kx(t))$$

In the above calculation v(t) represents the velocity at a certain time, m is the mass of the object, and a(t) represents the acceleration of the shape. This first half of the equation takes into account the moving shape and the second half accounts for the springs. Where the k term is the spring constant determined from tests conducted earlier specifically designed to find the value for the springs. And the x(t) term is the displacement at a certain time.

The next set of data analyzed was the RMS force value, which was calculated by,

$$F(t) = ma(t) + kx(t)$$

Where just as in the power equation the m and a(t) terms represent the force of the shape and the k and x(t) terms represent the force of the springs.

# 6. Conclusions and Recommendations

The optimal cross sectional shape for generating renewable energy from vortex induced vibrations is highly dependent upon the type of generator to be used. Different types of generators are complimented by different design components in an oscillating body when used in VIV energy generation. The larger forces produced by the “T” shapes would favor a generator which produces energy by applying torque to the system. A hydraulic generator could be considered with using “T” shapes as the oscillating body because they operate at high torques and low velocities. The cylinder produced much lower amplitudes and forces; however it generated much higher frequencies, favoring a low torque generator, or an electromagnetic generator which is more dependent upon the velocity and frequency of oscillations. Further work on this project will require a specific generator to be selected or designed prior to optimizing the cross sectional shape of the oscillating body.

## 6.1. Conclusions from Computer Simulations

Lift coefficients were compared when optimizing cross sectional shapes while running FEA computer simulations. The team found that sharper trailing edges lead to greater instances of vorticity while shapes with free stream geometries did not produce vortices with the same magnitude. We feel that this is because the sharper trailing edges left areas of low pressure, ideal to creating vortices. For example, a very evident comparison was simply reversing the orientation of a triangle. When a triangle was oriented with its vertex pointing upstream, it produced a lift coefficient of almost 1.5 at a Reynolds number of 5000. When the vertex was oriented downstream however, the lift coefficient was nearly 0. This principle continued when comparing round shapes such as circles and ellipses to “T” shapes.

It was also determined that a blunt leading edge created an area of decelerated flow that stored potential energy in front of the oscillating body. This energy was released as vortices were shed off of the trailing edge. This concept, called an adverse pressure gradient, (Scott, 2005) it often avoided to delay flow separation however, inducing flow separation encourages the creation of vortices. A higher pressure gradient creates a thicker boundary layer which leads to flow separation. After the flow separates, vortices will form in the area of low pressure directly downstream of the separation point. This can be seen when comparing the Triangular “T” shape resembling an arrow to the basic “T” shape. At a Reynolds number of 5000, the basic “T” shape produced a lift coefficient of 1.75 while the Triangular “T” only produced a lift coefficient of 0.80.

Using these two principles, variations of “T” shapes were explored finding that the basic “T” shape and the concave “T” shapes produced the largest lift coefficients. It was also found that adding the horizontal portion of the “T” seemed to aid in the formation of a more regulated von Kármán vortex street. This is hypothesized to produce more consistent oscillations in a wider range of variables.

## 6.2. Conclusions from Physical Testing

Physical tests mirrored the FEA testing conducted beforehand. The higher lift coefficients produced by the two “T” shapes lead to a 122% and a 108% percent increase in peak force at our maximum fluid velocity over the cylinder. The increase in peak force is also related to the 127% and 114% increase in oscillation amplitude observed in the “T” shapes at the same velocity when compared to the cylinder.

In contrast, the cylinder recorded frequencies 537% greater than the “T” shapes. This dramatic increase can be connected to difficulty in achieving the lock-in frequency of the cylinder. While the “T” shapes achieved the lock-in frequency, maintaining consistent oscillations with reasonably reliable data, the cylinder would oscillate with an inconsistent frequency with much smaller oscillations. This suggested that the mass of the cylinder may need to be changed, or different dampening springs with a different k value may be needed. These consistently higher frequencies lead to a dramatic increase in theoretical power density, approximately 150 times as great as the theoretical power densities of the two “T” shapes tested. This leads the team to believe that the recorded data was inconclusive and that further data collection must occur, specifically by revisiting the cylinder and achieving its lock-in frequency. One other conclusion that can be reached from the collection of physical data is that the “T” shapes performed more reliably than the cylinder at the low fluid velocities tested in this project. This is a fairly significant conclusion because the goal of energy generation from vortex induced vibrations is to target regions and bodies of water with lower fluid velocities, specifically around 2 to 3 knots.

## 6.3. Recommendations for Further Research

While much of the data collected was conclusive and in agreement with suspected results, there is much room for improvement in testing methods and problem formulation. The benefits of this technology call for continued research in the field. With the promise of renewable energy generation in low velocity fluid flow, significant effort should be taken to optimize the oscillating bodies and their efficiency of the system when including the generators. The following lists areas where further research and development can be focused.

The primary recommendation for further work in this area is to target a specific type of generator that will be used in each specific application. As stated previously, a low speed, high torque generator will favor shapes such as the "T" and the concave "T" which produce larger forces while a high speed, low torque generator will work more efficiently with a shape similar to the cylinder which generated significantly higher frequencies. Beginning with a specified generator will allow future teams to target specific design concepts when optimizing the cross sectional shape of the oscillating body.

Increasing the scale of physical tests may lead to increased validity. Current technologies deployed in the real world environment used 6" diameter cylinders while we were only able to test with 1" diameter cross sections. In order to facilitate larger testing, a prebuilt testing tank may be necessary. Finances and supplies limited the design of the test tank used in this project, however if access could be achieved to a testing tank similar to that used in the University of Michigan testing, there is the opportunity for a drastic increase in data reliability. One such test tank may be found in Alden Research Laboratory in Holden, MA. This facility focuses on computational fluid dynamics and has many testing setups that could test the optimization of the technology and even effects of the technology when implemented in a natural setting with their river research laboratory.

Increasing the scale of testing could affect the results in two very important ways. First, increasing the scale will lead to greater forces produced and more closely resemble those which a full scale system would produce. More importantly the increase in forces generated would not be matched by an increase in friction. A major design obstacle in this project was overcoming the large amounts of dynamic and static friction found in this small scale testing rig without access to a significant level of monetary resources. The friction produced in larger scale testing will play less of a role in the results collected.

If the scale of the testing is increased, there may also be a dramatic effect on the results gathered from the concave "T" shape. An increase in the height of the concave "T" will facilitate a larger radius on the trailing edge of the "T". This larger radius may contribute to the generation of stronger vortices, increasing the lift coefficient, peak forces, and therefore power density.

Finally, allowing all shapes to be tested within their lock-in frequency will significantly increase the correlations between the different shapes. Unfortunately the lock-in frequency will vary with the different geometries however; there are two proposed solutions to this problem. The first is to regulate the fluid flow so that the varying flow rates are specified by a percentage of each test shapes lock-in frequency range. This will be difficult because a more precise and flexible pump mechanism will be required. Also, this will mean that each shape will be tested at different fluid velocities so comparisons may not be as accurate or conclusive. The second solution is to vary the natural frequency of the cylinder. This can be done by either changing the damping spring which would alter the "k" value, or changing the mass of the cylinder so that the natural frequency of the cylinder more closely resembles that of the "T" shapes. Testing all of the shapes within their lock-inn frequency range will allow for increased validity.

# BIBLIOGRAPHY


Bernitas, M., Raghavan, K., Ben-Simon, Y., & Garcia, E. M. (2008). VIVACE (Vortex Induced Vibrations and Clean Energy): A New Concept of Clean and Renewable Energy from Fluid Flow. *Journal of Offshore mechanics and Artic Engineering*.

Chou, J. H., Miau, J.-i., Yang, C.-c., & Chen, T.-l. (1994, October 4). *Patent No. 5351559.* Taipei, Taiwan.

Dalton, C. (n.d.). *Fundamentals of Vortex-Induced Vibration.* Huston, Texas: University of Huston.

El Wahed, A. K., Johnson, M. W., & Sproston, J. L. (1993, October). Numerical Study of Vortex Shedding from Different Shaped Bluff Bodies. *Flow Measurement and Instrumentation, IV*(4), 233-240.

Georgia Tech. (n.d.). *Vortex Shedding*. Retrieved October 12, 2010, from Google: http://webcache.googleusercontent.com/search?q=cache:j3bRr9GHzKAJ:usli.gatech.edu/Docs-General/Vortex%2520Shedding.ppt+vortex+shedding+GATech&cd=1&hl=en&ct=clnk&gl=us

Graebel, W. P. (2007). *Advanced Fluid Mechanics.* Burlington, Massachusetts: Academic Press.

Green, S. I. (1995). *Fluid Vortices: Fluid Mechanics and its Applications.* The Netherlands: Kluwer Academic Publishers.

Hansen, S. O. (2007). Vortex Induced Vibrations. *Structural Engineers World Congress.* Bangalore, India.

Klamo, J. T. (2007). *Effects of Damping and Reynolds Number on Vortex Induced Vibration.* Pasadena: California Institute of Technology.

Madrigal, A. (2008, October 28). *Tapping the Vortex for Green Energy*. Retrieved October 2, 2010, from Wired Science: http://www.wired.com/wiredscience/2008/10/hidden-vortex-i/

Matsumoto, M., Shirato, H., Yagi, T., Shijo, R., Fguchi, A., & Tamaki, H. (2003). Effects of Aerodynamic Interferences Between Heaving and Torsional Vibration of Bridge Decks: The Case of Tacoma Narrows Bridge. *Journal of Wind Engineering and Industrial Aerodynamics*(91), 1547 - 1557.

Merzkirch, W. (2005). Vortex-Shedding Flow Metering Using Ultrasound. *Fluid Mechanics of Flow Metering*.

Scott, J. (2005, February 13). *Golf Ball Dimples & Drag*. Retrieved April 25, 2011, from AerospaceWeb: http://www.aerospaceweb.org/question/aerodynamics/q0215.shtml

U.S. Energy Information Administration. (n.d.). *Energy Sources*. Retrieved October 12, 2010, from U.S. Department of Energy: http://www.eia.doe.gov/kids/energy.cfm?page=2

Vortex Hydro Energy. (2010). *Home*. Retrieved October 12, 2010, from Vortex Hydro Energy: http://www.vortexhydroenergy.com/

*Water Flow in Tubes - Reynolds Number*. (n.d.). Retrieved October 13, 2010, from The Engineering Toolbox: http://www.engineeringtoolbox.com/reynold-number-water-flow-pipes-d_574.html

White, F. (2011). *Fluid Mechanics.* New York: McGraw Hill.

Wu, J.-Z., Ma, H.-Y., & Zhou, M.-D. (2006). *Vorticity and Vortex Dynamics.* Berlin, Germany: Springer.

# APPENDIX A: FREQUENCIES FOR VARIOUS LENGTH TO WIDTH RATIOS FOR A T SHAPPED VORTEXSHEDDER

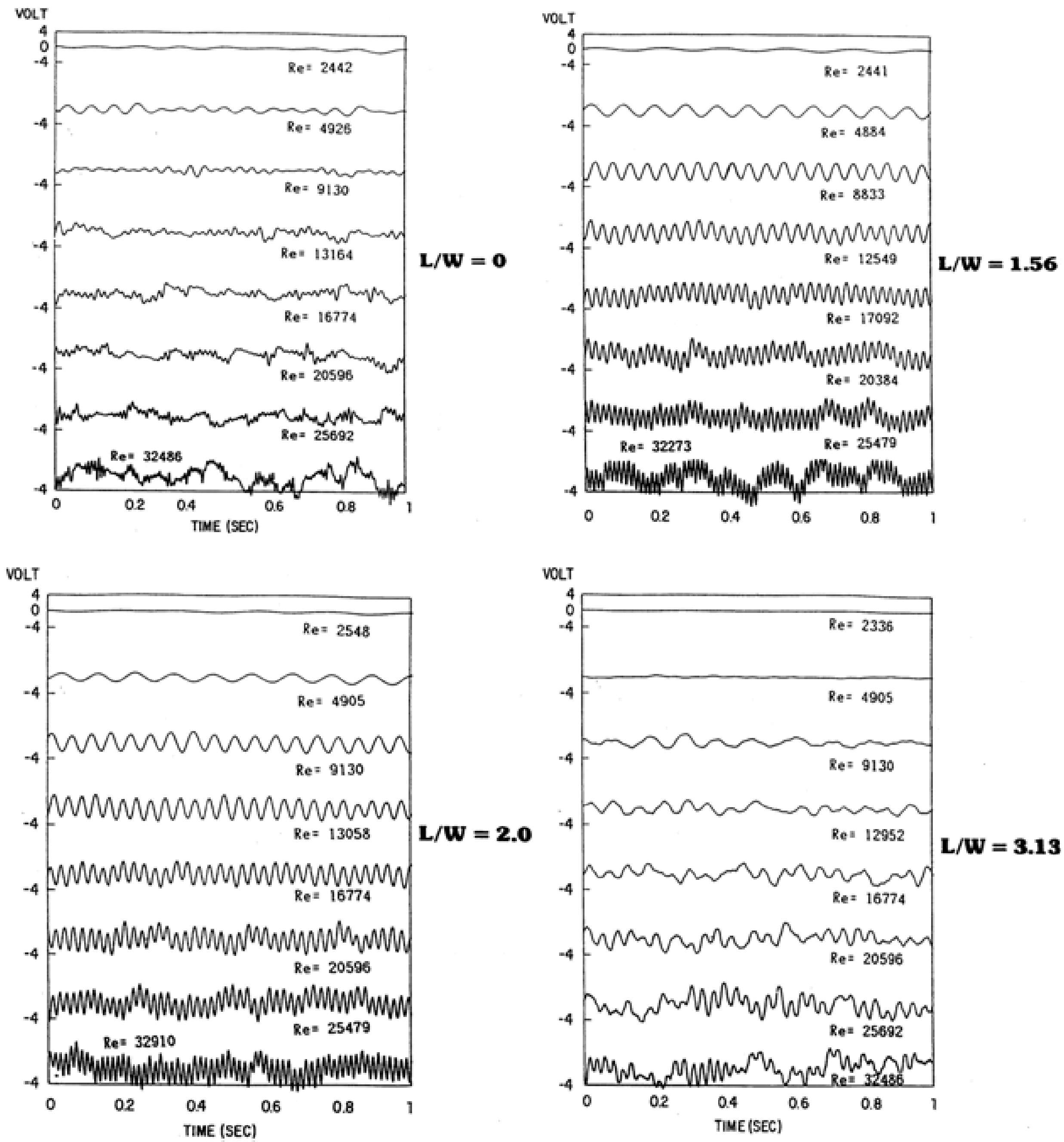

# APPENDIX B: PROPOSED TANK DESIGN

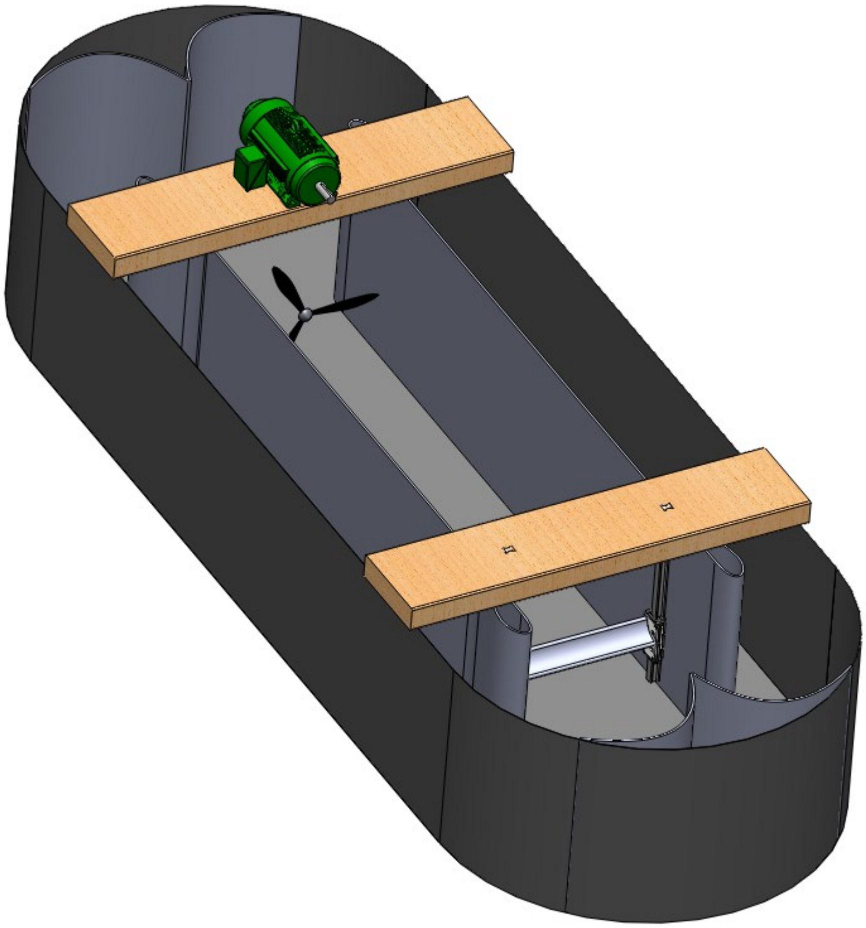

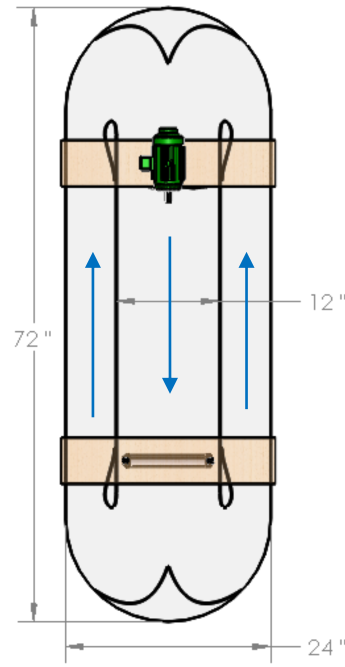


The blue arrows show the direction of flow in the tank.

This SolidWorks screen shot shows the preliminary design of the overall test tank layout. The propeller would be secured in place below the motor and connected to the motor by a chain or belt with a desired gear ratio. The distance from the propeller to the oscillating object would be 3 feet. The slides would be securely fastened (not as shown) in the position shown to keep them fixed during a fluid flow. Position detecting equipment could be mounted above the sliding mechanism on top of the 2x6.

# APPENDIX C: MATHCAD CALCULATIONS FOR STRESS AND DEFLECTION OF OSCILLATING RODS

Noryl (Polyphenylene Oxide (PPO)and Pol Polystyrene (PS)):

Inputs: $r := .5in$ — r = radius of rods

$E := .289 \cdot 10^{6} psi$ — E = Young's Modulus

$P := 2N$ — P = force exerted to end of rods (this force is a result of the bluff body in a fluid flow)

$l := 12in$ — l = the maximum length of the rods (from the bearings to the bluff body)

$I := 2\left(\frac{\pi r^{4}}{4}\right)$ — Multiplied by 2 because there is going to be 2 rods.

$$E \cdot I \cdot \frac{d^{2}}{dx^{2}} \nu = -P(l - x)$$

$$E \cdot I \cdot \left(\frac{d}{dx} \nu\right) = \frac{-P \cdot x \cdot (2l - x)}{2} + C_1$$

Slope at x=0 for a cantilever beam is 0, therefore C1=0.

Slope at x=12 inches:

$$\frac{d}{dx} \nu := \frac{-P \cdot l^{2}}{2 \cdot E \cdot I} = -0.065 \cdot deg$$

v = the deflection of ends of the rods. (its derivative will give the slope of the rod)

$$E \cdot I \cdot \nu = \frac{-P \cdot x^{2} \cdot (3l - x)}{6} + C_1 \cdot x + C_2$$

Deflection at x=0 for a cantilever beam is 0, therefore C2=0.

$$\nu = \frac{-P \cdot x^{2} \cdot (3l - x)}{6}$$

Deflection at x=12 inches:

$$\nu_{max} := -1 \cdot \frac{P \cdot l^{3}}{3E \cdot I}$$

$$\nu_{max} = -9.128 \times 10^{-3} \cdot in$$

$$\sigma_{max} := \frac{P \cdot l \cdot r}{I}$$

$$\sigma_{max} = 0.027 \cdot ksi$$

$\sigma_{Yield} := (6.5 - 7.1)ksi$ — $\sigma_{yield}$ = the yield stress of the rods

The calculations shown above are for Noryl (the material selected). These calculations were reiterated for every material considered and for various radii by changing the values highlighted in red.

# APPENDIX D: FINAL TANK DESIGN

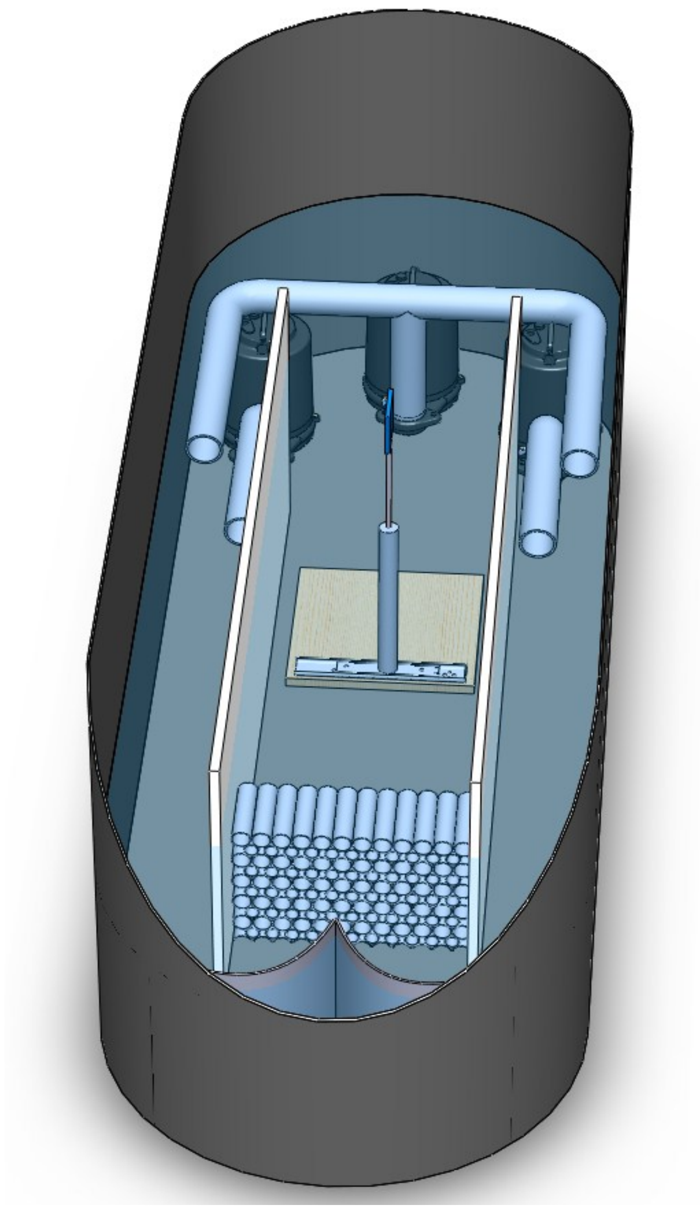

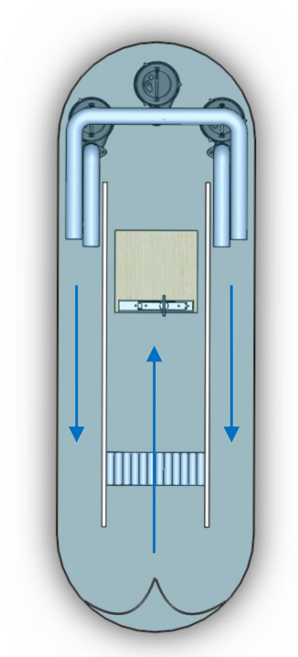

The blue arrows show the direction of flow in the tank.

This SolidWorks screen shot shows the overall test tank layout. The pumps pump the water down the outer channels, where the water merges from the converger and travels through the diffuser. The water is then fairly uniform at the testing area.

# APPENDIX E: A TABLE USED IN THE MATERIAL SELECTION PROCESS FOR THE OSCILLATING RODS

| Plastic Type | | | % Fill Composition | Density Range (lb/in^3) | | Price Range ($/lb) | | Young's Modulus Range (10^6 psi) | | Yeilding Strength Range (ksi) | |
|---|---|---|---|---|---|---|---|---|---|---|---|
| Name | Abrev. | Common Name | | Low | High | Low | High | Low | High | Low | High |
| **Acrylonitrile Butadiene Styrene** | **ABS** | | **Extrusion** | **0.0368** | **0.0390** | **$0.84** | **$0.92** | **0.290** | **0.421** | **4.3** | **6.4** |
| Polyoxymethylene | POM | Acetal/Delrin | Homopolymer | 0.0509 | 0.0517 | $1.51 | $1.72 | | | | |
| High Density Polyethylene | HDPE | Range | | 0.0339 | 0.0349 | $0.67 | $0.92 | 0.090 | 0.158 | 2.6 | 4.5 |
| Low Density Polyethylene | LDPE | | Molding and Extrusion | 0.0331 | 0.0337 | $0.69 | $0.76 | 0.025 | 0.041 | 1.3 | 2.1 |
| Polyvinylidene Flouride | PVDF | Kynar | Homopolymer | 0.0639 | 0.0643 | $7.49 | $12.00 | | | | |
| **Polyphenylene Oxide / Polyamide Alloy** | **PPO/PA** | **Noryl** | **Unfilled** | **0.0394** | **0.0401** | **$2.14** | **$2.36** | **0.289** | **0.315** | **6.5** | **7.1** |
| **Polyamide** | **PA** | **Nylon** | **Unfilled (Type 12)** | **0.0365** | **0.3680** | **$3.18** | **$3.50** | **0.174** | **0.203** | **3.0** | **6.1** |
| Polybutylene Terephthalate | PBT | | General Purpose | 0.0470 | 0.0499 | $1.22 | $1.34 | | | | |
| Polyetheretherketone | PEEK | | Unfilled | 0.0470 | 0.0477 | $46.80 | $53.90 | | | | |
| Polycarbonate | PC | | High Viscosity | 0.0430 | 0.0437 | $1.33 | $1.71 | | | | |
| **Polystyrene** | **PS** | | **General Purp.** | **0.0376** | **0.0379** | **$0.61** | **$0.67** | **0.331** | **0.476** | **4.2** | **6.0** |
| Polysulfone | PSU | | Extrusion | 0.0444 | 0.0452 | $6.50 | $7.49 | | | | |
| Polyphenylene sulfide | PPS | | Unfilled | 0.0484 | 0.0491 | $8.45 | $10.40 | | | | |
| Amorphous Polyamide/imide | PAI | Torlon | Unfilled | 0.0506 | 0.0524 | $23.00 | $25.20 | | | | |
| Ultra High Molecular Weight Polyethylene | UHMW | | Molding and Extrusion | 0.0336 | 0.0343 | $1.22 | $1.52 | 0.130 | 0.140 | 3.1 | 4.0 |
| Polyetherimide | PEI | Ultem | Unfilled | 0.0455 | 0.0462 | $6.40 | $7.05 | | | | |
| Polyimide Resin | PI | Vespel | Unfilled | 0.0480 | 0.0517 | $17.90 | $20.70 | | | | |
| | | | | Water: | 0.0360 | | | | | | |

# APPENDIX F: A TABLE OF FLOW SPEED RESULTS THAT MAPS THE VELOCITY PROFILE FOR DIFFERENT PUMP CONFIGURATIONS

| AVERAGE VELOCITIES USING 1/3 HORSEPOWER PUMP (meters/second) | | | | | |
|---|---|---|---|---|---|
| | LEFT 1 | LEFT 2 | MIDDLE | RIGHT 2 | RIGHT 1 |
| TOP | 0.12 | 0.22 | 0.25 | 0.20 | 0.16 |
| CENTER | | | 0.24 | | |
| BOTTOM | 0.03 | 0.11 | 0.19 | 0.10 | 0.01 |

| AVERAGE VELOCITIES USING 1/2 HORSEPOWER PUMP (meters/second) | | | | | |
|---|---|---|---|---|---|
| | LEFT 1 | LEFT 2 | MIDDLE | RIGHT 2 | RIGHT 1 |
| TOP | 0.27 | 0.32 | 0.33 | 0.27 | 0.18 |
| CENTER | | | 0.30 | | |
| BOTTOM | 0.16 | 0.27 | 0.32 | 0.29 | 0.19 |

| AVERAGE VELOCITIES USING 5/6 HORSEPOWER PUMP (meters/second) | | | | | |
|---|---|---|---|---|---|
| | LEFT 1 | LEFT 2 | MIDDLE | RIGHT 2 | RIGHT 1 |
| TOP | 0.38 | 0.41 | 0.42 | 0.39 | 0.22 |
| CENTER | | | 0.39 | | |
| BOTTOM | 0.21 | 0.34 | 0.39 | 0.37 | 0.27 |